

1

2 **Modeling kidney development, disease, and plasticity 3 with clonal expandable nephron progenitor cells 4 and nephron organoids**

5

6 Biao Huang^{1,2,10}, Zipeng Zeng^{1,2,10}, Hui Li¹, Zexu Li³, Xi Chen², Jinjin Guo², Chennan C. Zhang^{1,2},
7 Megan E. Schreiber^{1,2}, Ariel C. Vonk^{1,2}, Tianyuan Xiang^{1,2}, Tadrushi Patel^{1,2}, Yidan Li^{1,2}, Riana K.
8 Parvez², Balint Der², Jyun Hao Chen^{1,2}, Zhenqing Liu⁸, Matthew E. Thornton⁴, Brendan H.
9 Grubbs⁴, Yarui Diao⁵, Yali Dou⁶, Ksenia Gnedeva^{2,7}, Nils O. Lindström², Qilong Ying², Nuria M.
10 Pastor-Soler¹, Teng Fei³, Kenneth R. Hallows¹, Andrew P. McMahon², and Zhongwei Li^{1,2,9,*}

11

12 ¹USC/UKRO Kidney Research Center, Division of Nephrology and Hypertension, Department of Medicine,
13 Keck School of Medicine, University of Southern California, Los Angeles, CA 90033, USA

14 ²Department of Stem Cell Biology and Regenerative Medicine, Keck School of Medicine, University of
15 Southern California, Los Angeles, CA 90033, USA

16 ³College of Life and Health Sciences, Northeastern University, Shenyang 110819, P. R. China

17 ⁴Division of Maternal Fetal Medicine, Keck School of Medicine, University of Southern California, Los An-
18 geles, CA 90033, USA

19 ⁵Department of Cell Biology, Duke University School of Medicine, Durham, NC 27710, USA.

20 ⁶Department of Medicine, Department of Biochemistry and Molecular Medicine, University of Southern Cal-
21 ifornia, CA 90033, USA

22 ⁷Tina and Rick Caruso Department of Otolaryngology-Head and Neck Surgery, University of Southern Cal-
23 ifornia, Los Angeles, CA 90033, USA

24 ⁸Division of Stem Cell Biology Research, Department of Developmental and Stem Cell Biology, Beckman
25 Research Institute of City of Hope, Duarte, CA 91010, USA.

26 ⁹Lead contact

27 ¹⁰These authors contributed equally

28

29 *Correspondence: zhongwei.li@med.usc.edu

30

1 **SUMMARY:**

2 Nephron progenitor cells (NPCs) self-renew and differentiate into nephrons, the functional units
3 of the kidney. Here we report manipulation of p38 and YAP activity creates a synthetic niche that
4 allows the long-term clonal expansion of primary mouse and human NPCs, and induced NPCs
5 (iNPCs) from human pluripotent stem cells. Cultured iNPCs resemble closely primary human
6 NPCs, generating nephron organoids with abundant distal convoluted tubule cells, which are not
7 observed in published kidney organoids. The synthetic niche reprograms differentiated nephron
8 cells into NPC state, recapitulating the plasticity of developing nephron *in vivo*. Scalability and
9 ease of genome-editing in the cultured NPCs allow for genome-wide CRISPR screening, identi-
10 fying novel genes associated with kidney development and disease. A rapid, efficient, and scal-
11 able organoid model for polycystic kidney disease was derived directly from genome-edited NPCs,
12 and validated in drug screen. These technological platforms have broad applications to kidney
13 development, disease, plasticity, and regeneration.

14

1 INTRODUCTION

2 $SIX2^+$ nephron progenitor cells (NPCs) play a central role in kidney organogenesis^{1,2}. In the de-
3 veloping kidney, niche signals coordinate two different NPC fates: some NPCs are induced to
4 form nephrons, the functional units of the kidney, while others self-renew to repopulate the pro-
5 genitor pool³. NPCs are then exhausted shortly after birth in the mice and before birth in humans,
6 leaving limited regenerative potential in adult mammalian kidneys. Dysregulation of NPC fates
7 underlies a number of congenital kidney diseases⁴ while uncontrolled proliferation of NPCs in
8 Wilms tumor is the most prevalent pediatric kidney cancer⁵. Thus, a deeper insight into NPC bi-
9 ology is central to improving an understanding of kidney development, congenital disease and
10 cancer, and to applying developmental insight to regenerating kidney functions.

11 Over the past few years, we and others have developed systems to either generate NPCs
12 *de novo* from pluripotent stem cells or expand NPCs from primary NPCs isolated from embry-
13 onic/fetal kidneys such that: 1) mouse and human NPC-like cells can now be generated transi-
14 ently using step-wise directed differentiation protocols from mouse and human pluripotent stem
15 cells (hPSCs)⁶⁻⁹; 2) primary mouse and human NPCs can be isolated and expanded for a short
16 period of time in two-dimensional (2D) culture format^{10,11} or expanded long term over a few months
17 in our previously reported three-dimensional (3D) culture format¹². These systems have advanced
18 our current understanding of NPC biology, and NPC-derived nephron organoids have been shown
19 to be powerful tools in modeling kidney development and diseases¹³.

20 While acknowledging progress, significant limitations remain. First, current hPSC-derived
21 nephron organoids fail to generate mature and functional kidney cell types and lack a diversity of
22 critical cell types characteristic of distal nephron segments¹³⁻¹⁶, likely reflecting the quality of
23 hPSC-derived NPC-like cells¹⁶. Second, compared to 2D culture, the currently available NPC 3D
24 culture system is tedious and less compatible with functional genomics tools, such as CRISPR
25 screens¹⁷⁻¹⁹, hindering genomic scale study of NPC biology. Third, despite attempts from us and

1 others^{10,12,20}, it has not been possible to expand NPCs derived from hPSCs, the desired cell
2 source for kidney regeneration and disease modeling, over the long term.

3 Here, we report the development of chemically-defined 2D culture systems supporting the
4 stable clonal expansion, over several months, of primary mouse and human NPCs, and hPSC-
5 derived NPCs. In this system, NPCs maintain NPC properties and differentiate to generate distal
6 cell types refractory to previous kidney organoid models. The novel NPC system facilitates ge-
7 nome-scale genetic screening, disease modeling and provides a scalable platform for drug dis-
8 covery.

9

10 RESULTS

11 p38 inhibition allows the derivation of clonal expandable NPC lines from any mouse strain.

12 We previously developed a 3D culture system that can expand mouse NPCs (mNPCs) as clusters
13 of cells in a chemically-defined culture medium, mNPSR¹². However, mNPSR did not support
14 mNPC expansion in a regular monolayer (2D) culture setting. To solve this problem, we have
15 systematically screened the addition of a variety of small molecules and growth factors to mNPSR
16 medium, resulting in mNPSR-v2: a chemically-defined medium that supports the derivation and
17 long-term clonal expansion of mNPC lines from multiple mouse strains (**Fig. 1A**, **Fig. S1A** and
18 **Tables S1 and S2**).

19 Compared to mNPSR, mNPSR-v2 has four additional small molecules: SB202190 (inhib-
20 itor of p38 MAPK), DAPT (inhibitor of Notch signaling), A83-01 (inhibitor of TGF- β signaling) and
21 LDN193189 (inhibitor of BMP signaling), and required a different concentration (1.5 μ M) of
22 CHIR99021 (inhibitor of GSK3). Of these additional components, we have previously found that
23 adding A83-01 and LDN193189 to mNPSR can enable the expansion of mNPCs at lower seeding
24 mNPC numbers in a 3D culture setting²¹. LDN193189¹⁰ and DAPT¹¹ have also been used in sup-
25 porting short-term expansion of mNPCs. Consistently, we also noticed that adding DAPT pre-
26 vented spontaneous differentiation from the 2D cultured mNPCs (**Fig. S1C and D**). The p38

1 MAPK inhibitor SB202190 has not been previously reported to support mNPC self-renewal. Inter-
2 estingly, adding SB202190 appears to have the most significant effect in sustaining the percent-
3 age of SIX2⁺/PAX2⁺ mNPCs in culture (**Fig. 1B and S1B**). Importantly, phosphorylated p38 (p-
4 p38), the active form of p38 MAPK, was not detected in primary mNPCs (**Fig. 1C**), indicating an
5 intrinsic inhibition of p38 MAPK activity in the self-renewing mNPCs *in vivo*. mNPCs expanded in
6 mNPSR-v2 stably proliferate with highly homogeneous morphology (**Fig. 1D and E**). After 4
7 weeks of culture and more than 10 passages, more than 95% of the cultured mNPCs are triple
8 positive for SIX2/PAX2/ITGA8 and SALL1/WT1/ITGA8 (**Fig. 1F and G**). qRT-PCR showed the
9 NPC marker genes, *Six2*, *Sall1*, *Pax2*, *Wt1* and *Gdnf*, were expressed at similar levels to those
10 observed in primary NPCs (**Fig. S1E**). Upon withdrawing each individual medium component from
11 mNPSR-v2, we confirmed that all components are essential to maintain the proper growth rate
12 and undifferentiated state of the mNPCs (**Fig. S1F and G**).

13 We then utilized various assays to examine the nephrogenic potential of the cultured
14 mNPCs *in vitro* and *in vivo*. When cultured mNPCs were aggregated and placed in close contact
15 with the dorsal side of an isolated E12.5 spinal cord, a classic inducer of NPC development^{6,12},
16 we observed dramatic morphological changes, leading to the formation of numerous tubule-like
17 structures after 7 days (**Fig. 1H**). Immunostaining further confirmed the formation of PODXL⁺ glo-
18 meruli, LTL⁺ proximal tubule, and CDH1⁺ distal tubule structures upon spinal cord induction (**Fig.**
19 **1I**). Nephron organoids were also formed from cultured mNPCs using our chemically-defined as-
20 say¹², generating multiple segments of the nephron (**Fig. S1H**). When we reconstructed an engi-
21 neered kidney from cultured mNPCs and cultured ureteric bud (UB)²², mNPCs induced dramatic
22 branching morphogenesis from the UB (**Fig. S1I**), while the UB induced nephron formation from
23 the mNPCs (**Fig. S1J**). Further, when mNPCs were transplanted onto the chicken chorioallantoic
24 membrane (CAM) *in vivo*²³, mNPCs differentiated into nephrons and chick vasculature infiltrated
25 the transplant (**Fig. S1K-M, and Video S1**).

1 In strong contrast to the 3D-cultured mNPCs, which can be expanded only as clusters of
2 cells^{12,21}, 2D-cultured mNPCs were efficiently expanded from single cells with a high cloning effi-
3 ciency of 60–70% (**Fig. 1J-M**), with retention of NPC gene expression and nephrogenic potential
4 for at least 2 months (**Fig. 1N, S2A and B**). To compare the global gene expression of cultured
5 and primary mNPCs^{12,24}, we performed bulk RNA-seq (**Table S3**). Based on principal component
6 analysis (PCA), cultured NPCs were clustered tightly together, with a clear separation of cultured
7 and primary NPCs from the SIX2-negative non-NPCs along the PC1 axis (**Fig. 1O and S2C**).
8 Importantly, cultured mNPCs largely overlapped with primary E11.5, E12.5, and E13.5 mNPCs in
9 PC1 and PC3 axes (**Fig. S2D**). Consistently, cultured mNPCs were clustered with these early-
10 stage mNPCs in the heatmap, using a selective group of typical NPC and nephron marker genes
11 (**Fig. 1P**). These results suggest that cultured mNPCs likely represent early-stage (E11.5 to E13.5)
12 mNPCs. Furthermore, the robustness of mNPSR-v2 allowed us to derive mNPC lines from iso-
13 lated E11.5 metanephric mesenchyme (**Fig. S2E and F**) or from whole kidney cells of an early
14 embryonic kidney (**Fig. S2G-K**), thus enabling the derivation of mNPC lines from any mouse strain
15 (**Fig. 1A and Table S4**).

16

17 **Capture the plasticity of developing nephron cells with mNPSR-v2 medium.**

18 While developing the mNPSR-v2 medium, we made an unexpected but interesting finding—a
19 significant portion (10–20%) of *Six2*-GFP[−] cells isolated from dissociated kidneys at all stages
20 (E12.5, E14.5, E16.5 and P0 kidneys) adopted a SIX2⁺/SALL1⁺ phenotype within 4 days of culture
21 (**Fig. 2A and B**). This finding suggests the possibility of phenotypic plasticity on the part of non-
22 NPC type(s) in mNPSR-v2 medium. To verify this observation, we excluded first the possibility of
23 potential contamination of a small number of *Six2*-GFP⁺ mNPCs in the *Six2*-GFP[−] population dur-
24 ing FACS. For this purpose, we confirmed the reported loss of SIX2⁺ NPCs in the postnatal day
25 3 (P3) kidney^{1,2} (**Fig. S3A**) and cultured dissociated single P3, P4, P5 and P7 kidney cells in
26 mNPSR-v2 for 4 days, and examined SIX2/SALL1 by immunostaining. Approximately 17% of the

1 P3 kidney cells and 7% of the P4 kidney cells were scored as *SIX2*⁺/*SALL1*⁺, rare *SIX2*⁺/*SALL1*⁺
2 cells were observed also within P5 and P7 cultures (**Fig. 2C and D, and S3B and C**). These
3 results support the contention that a non-NPC-like cell-type generates *SIX2*⁺/*SALL1*⁺ NPC-like
4 cells under mNPSR-v2 condition. The reprogramming is most efficient in mNPSR-v2 (18%), less
5 efficient in mNPSR (6%), and does not happen in basal medium with 10% FBS (0%) (**Fig. S3D**
6 **and E**), suggesting that, in addition to the intrinsic plasticity of the cells, proper extrinsic signals
7 are also needed for successful reprogramming. To further characterize the induced *Six2*⁺ cells,
8 we developed an assay to purify these cells using an NPC lineage tracing reporter system³ (**Fig.**
9 **2E**). P3 kidneys were isolated from *Six2*-GFP-CreERT2; *Rosa26*-tdTomato (*Six2*-tdT for short)
10 mice, dissociated into single cells, and cultured in mNPSR-v2. Three days after culture, tamoxifen
11 was added, which allows the permanent labeling of tdTomato (tdT) in cells that express *Six2*.
12 After another 24 hours (on day 4 of culture), similar to immunostaining results, around 20% of the
13 cultured P3 kidney cells became *Six2*-tdT⁺ as shown by FACS (**Fig. S3F and G**). Upon additional
14 culture to day 8, these *Six2*-tdT⁺ cells showed a more complete NPC profile expressing *Six2*,
15 *Pax2*, *Sall1*, *Wt1*, *Gdnf*, *Hoxd11*, and *Eya1*, coinciding with loss of expression of nephron marker
16 genes *Slc12a1*, *Slc12a3*, and *Aqp1* (**Fig. 2F**). Taken together, these data suggest that some kid-
17 ney cell types retain a developmental plasticity to convert to NPCs for a limited period following
18 the cessation of active nephrogenesis, and these cells were reprogrammed to NPC-like cells in
19 mNPSR-v2 culture.

20 *Wnt4*⁺ cells, the immediate differentiated progenies of the NPCs, can migrate back to the
21 cap mesenchyme niche, where NPCs reside, and reverse back to the NPC state *in vivo*²⁵. To
22 investigate whether *Wnt4*⁺ cells might also contribute to the plasticity we observed *in vitro*, we
23 injected tamoxifen into P2 *Wnt4*-GFP-Cre-ERT2; *Rosa26*-tdTomato (*Wnt4*-tdT for short) mice to
24 permanently label *Wnt4*⁺ cells and their progeny. Kidneys were isolated 24hrs later on P3, and
25 tdTomato⁺ cells FACS purified and cultured in mNPSR-v2 (**Fig. 2G and H**). After 4 days of culture,
26 more than 70% of the cultured *Wnt4*-tdT⁺ cells stained positive for *SIX2*/*SALL1*, as compared to

1 20% starting from P3 whole kidneys (**Fig. 2I and J**). These results suggest that, like *in vivo*, the
2 *Wnt4*⁺ cells represent a highly plastic cell population that can be efficiently reprogrammed to an
3 NPC state *in vitro*. It also further strengthened the notion that the mNPSR-v2 medium represents
4 a *bona fide* synthetic niche that allows NPC self-renewal and *Wnt4*⁺ cells lineage reprogramming
5 as *in vivo*.

6
7 **Genome-wide CRISPR screen in the NPC lines identify functional genes for kidney devel-**
8 **opment and disease.**

9 The ease of generating CRISPR/Cas9 sgRNAs has afforded the development of CRISPR tech-
10 nologies for pooled genome-wide screens¹⁷⁻¹⁹, enabling the interrogation of functional genes in
11 the whole genome for the discovery of novel insights into biological processes and the identifica-
12 tion of novel drug targets and therapies for diseases²⁶.

13 Considering the central roles NPCs play in kidney organogenesis, Wilms tumor, and con-
14 genital kidney diseases such as congenital anomalies of the kidney and urinary tract (CAKUT),
15 the use of CRISPR screen tools to understand NPC biology from the genome-wide perspective
16 could provide valuable molecular and genetic insight into these areas. Thus, as a proof-of-concept,
17 we introduced a genome-wide CRISPR knockout library²⁷ into cultured NPCs to screen for genes
18 essential for NPC fitness (**Fig. 3A**). Abundance of sgRNAs in the cultured NPCs were determined
19 by next-generation sequencing 3 weeks after CRISPR library was introduced (**Tables S5**). Com-
20 pared to sgRNA abundance in the original CRISPR screen library, decrease of sgRNA abundance
21 indicates that expressing the sgRNA results in gene knockout that reduces cell fitness (e.g., en-
22 hanced NPC apoptosis or reduced NPC proliferation), while conversely, increase of sgRNA abun-
23 dance indicates increased fitness upon gene removal (e.g. blocked apoptosis or differentiation,
24 or enhanced NPC proliferation). With the MAGeCK-VISPR tool²⁸, sgRNA abundance changes
25 from 4 different sgRNAs targeting the same gene in the library are statistically integrated as beta

1 scores (**Table S6**). Positively-selected (i.e. increased sgRNA abundance) genes with more dra-
2 matic sgRNA abundance increase will have higher positive beta scores; while negatively-selected
3 genes with more dramatic sgRNA abundance decrease appear as lower negative beta scores.

4 Two biological replicates of this CRISPR screen showed high similarity overall (**Fig. S4A**).
5 As expected, significant global changes of sgRNA abundance were observed after 3 weeks of
6 the screen, with similar abundance for all sgRNAs in the library before the screen, and dispersed
7 distribution of the abundance of different sgRNAs after the screen (**Fig. S4B and S4C**). As ex-
8 pected, “pan-essential genes” in CRISPR knockout screens which include ribosomal and cell cy-
9 cle regulatory genes²⁹, underwent significant negative selection (**Fig. 3B**). Statistical analysis
10 (beta scores >1.5 or <-1.5) identified 410 positively-selected genes and 696 negatively-selected
11 genes shared between replicate assays (**Fig. 3C**).

12 Next, we used Ingenuity Pathway Analysis (IPA) to analyze identified gene sets (**Table**
13 **S7**). Consistent with the large number of essential genes identified in this type of screen, funda-
14 mental cellular pathways necessary for cell survival, such as basic transcription and translation
15 machineries, were found to be at the top of the enriched pathways from IPA’s Canonical Pathways
16 analysis. Importantly, mTOR signaling, microRNA biogenesis, and oxidative phosphorylation
17 pathways, which play critical roles in NPC self-renewal in *in vivo* studies³⁰⁻³⁴, were all identified
18 among the top enriched pathways in both replicates (**Fig. 3D, S4D and E, and Table S8**). Con-
19 sistent with the essential role of FGF signaling in NPC self-renewal *in vitro* (**Fig. S1F and G**) and
20 *in vivo*^{1,2}, *Fgfr1*, *Grb2*, *Mapk1*, and *Myc*, genes encoding critical FGF receptor, signaling mediator,
21 and effector proteins, were among the top negatively-selected genes (**Fig. 3E, and Table S9**).
22 On the contrary, *Dusp6*, which encodes a phosphorylase that inhibits FGF signaling in a feedback
23 loop, was a top positively-selected gene (**Fig. 3E**). *Mapk14*, which encodes p38 MAPK, was
24 among the top positively-selected genes, consistent with our observation that p38 inhibition is
25 essential for NPC self-renewal (**Fig. 1B and C, S1B, F and G**). Similar patterns were evident for

1 Wnt and LIF signaling pathway components (**Fig. S4F and G, and Table S9**). These results fur-
2 ther validated the high quality of our CRISPR screen results.

3 We next set out to systematically identify potential NPC self-renewal genes in the whole
4 genome from our CRISPR screen datasets. To further narrow down functional genes, we cross-
5 referenced our previously published bulk RNA-seq datasets for primary NPCs from various de-
6velopmental stages^{12,24}. First, we removed essential genes from the CRISPR screen hits. Second,
7 we removed the genes that showed low gene expression levels in the primary NPCs. Third, we
8 overlapped our CRISPR screen identified gene list with two NPC-enriched gene lists—E12.5
9 *Six2*⁺ NPC vs. *Six2* non-NPC¹² and E16.5 NPC vs. IPC (interstitial progenitor cell)²⁴. With this
10 stringent data filtration method, a short-list of 64 genes were obtained that showed consistent
11 results from both screen replicates (**Table S10**). Interestingly, 25 out of the 64 genes encode
12 proteins that localize to the nucleus (**Fig. 3F**). Among these genes, we identified *Sall1*³⁵⁻³⁷, *Wt1*³⁸,
13 *Foxc1*³⁹, and *Myc*^{40,41} as top negatively-selected genes, which are well-established transcription
14 factors for maintaining NPC identity *in vivo*. Genes with previously unknown functions in NPC self-
15 renewal were also identified. As an example, *Sobp* is a transcription factor known to regulate
16 cochlear development⁴². It is also expressed in the NPCs^{12,24}, with its expression dramatically
17 decreased in P0 NPCs, as compared to NPCs at earlier developmental stages. A recent study
18 reported that, *Sobp*, as a co-factor for *Six1*, interferes with the transcriptional activation of
19 *Six1/Eya1* target genes during craniofacial development, likely leading to Branchio-oto-renal syn-
20 drome (BOR)⁴³. These observations, together with our CRISPR screen result, support a role for
21 *Sobp* in the regulation of NPC fates.

22 Wilms tumor, the most prevalent pediatric kidney cancer, is associated with the retention
23 and expansion of cells that have overlapping signatures between NPCs and their early nephron-
24 committed descendants. Currently, around 30 Wilms tumor-related genes have been well estab-
25 lished⁵. Of note, 11 out of the 30 genes (36.7%) were identified by our CRISPR screen. The tumor

1 suppressor genes *Trp53* and *Bcor* were among the top positively selected genes, while onco-
2 genes such *Mycn* and *Max* were amongst the negatively selected gene set (**Fig. 3G, and Table**
3 **S11**). Dysregulation of normal kidney development process can also lead to congenital kidney
4 diseases, such as CAKUT, for which around 330 genes might be related⁴. Out of the 330 genes,
5 25 (7.6%), were identified in our CRISPR screen, consistent with the notion that dysregulation of
6 NPC fates represents a significant source for kidney malformation (**Fig. 3H and Table S11**). Con-
7 firmation of the large numbers of known Wilms tumor and CAKUT related genes suggests that
8 our CRISPR screen datasets might identify other genes with previously unknown functions in
9 these diseases (**Table S7**).

10 Epigenetic mechanisms have been found to play critical roles in stem/progenitor cell fate
11 decisions^{44,45}, including NPC self-renewal *in vivo*⁴⁶. Our CRISPR screen has identified the majority
12 of these reported epigenetic factors, including *Hdac1*⁴⁷, *Chd4*⁴⁸, *Ezh2*⁴⁹, and *Smarca4*⁵⁰. In addi-
13 tion, two other epigenetic regulators, *Kmt2a* (*Mll1*) and *Kat6a*, were found to be top negatively-
14 selected genes, whose function has not been examined in NPCs (**Fig. 3I-K**). Interestingly, recent
15 whole-exome sequencing in families with CAKUT identified dominant monogenic point mutations
16 in human *KMT2D* and *KAT6B* genes to cause syndromic CAKUT⁵¹. Thus, we were intrigued to
17 validate experimentally whether perturbations of *Kmt2a* and *Kat6a* in mouse NPCs can lead to
18 dysregulation of NPC fates. mNPCs treated with two small molecule inhibitors to KMT2A, MLL1
19 (inh), and WDR5 degrader⁵², and two small molecule inhibitors to KAT6A, WM-1119, and MOZ-
20 IN-3, showed significantly reduced proliferation, and decreased expression of NPC marker genes
21 SIX2, PAX2, SALL1, and WT1, linking KMT2A and KAT6A activities to the maintenance of NPC
22 identity (**Fig. 3L and M, and S4H and I**). These findings suggest mutations in *KMT2D* and *KAT6B*
23 might dysregulate NPC programs in association with human CAKUT .

24 Taken together, our CRISPR screen datasets (**Tables S5-S11**) provide valuable genome-
25 scale resources for future studies of kidney development, Wilms tumor, and CAKUT.

26

1 **Rapid, efficient, and scalable PKD modeling directly from genome-edited mouse NPCs.**

2 The long-term clonal expansion ability of the cultured NPCs, coupled with the ease of genome-
3 editing in 2D culture, encouraged us to explore genetic modeling of kidney disease. Autosomal-
4 dominant polycystic kidney disease (ADPKD) is the most prevalent inherited kidney disease oc-
5 curring at a frequency of approximately 1 in 500 live births⁵³. ADPKD patients develop large cysts
6 in their kidneys, which can frequently lead to end-stage kidney disease. There are limited effective
7 therapeutic options for patients with ADPKD. Studies from several groups⁵⁴⁻⁵⁸ have successfully
8 modeled ADPKD through the genetic removal of *PKD1* or *PKD2* in human pluripotent stem cells
9 (hPSCs), and PSC differentiation to cyst-forming kidney organoids, under a variety of conditions.

10 We designed a one-vector multiplexed CRISPR-Cas9 system, comprising three sgRNA
11 expression cassettes cloned in tandem into a basic lentiviral vector expressing a puromycin re-
12 sistance gene, for highly efficient one-step gene knockout directly in NPCs (**Fig. 4A**). The three
13 sgRNAs target the same gene with sgRNA targeting sequences 50-100 bp apart from each other
14 for increased gene knockout efficiency⁵⁹. Using a mouse NPC line constitutively expressing Cas9
15 and GFP (Cas9-GFP)⁶⁰ (**Table S4**), targeting with lentivirus expressing multiplexed sgRNAs
16 against *EGFP* led to near complete loss of EGFP fluorescence in NPCs (**Fig. 4B and C**).

17 We then generated *Pkd1* or *Pkd2* knockout NPCs using this system. All the genome-ed-
18 ited mNPC lines showed stable expression of NPC marker genes at similar levels to that of pri-
19 mary NPCs (**Fig. 4D**). Immunoblot analysis of the bulk *Pkd2*^{-/-} mNPCs confirmed that polycystin
20 2 (PC2, the protein product of *Pkd2*) was completely depleted (**Fig. 4E**). We next isolated single
21 cell clones from *Pkd1* or *Pkd2* bulk knockout mNPCs (**Fig. S5A**) and randomly selected *Pkd2*^{-/-}
22 clones #2, #4, and #5 and *Pkd1*^{-/-} clone #1 for further studies. All these clonal NPC lines showed
23 stable expression of NPC marker genes similar to primary NPCs (**Fig. S5B**). Targeted PCR flank-
24 ing the sgRNA targeting areas of the genome indicated deletions around the genomic loci (**Fig.**
25 **S5D**). Sanger sequencing confirmed genome editing resulted in premature termination of gene

1 transcription (**Fig. S5C**), and immunoblotting confirming the complete depletion of PC2 in all the
2 clonal *Pkd2*^{-/-} mNPC lines (**Fig. 4F**).

3 To examine cyst formation, we used our published protocol to make nephron organoids
4 at the air-liquid-interface in Transwells¹², then manually dissected organoids into smaller pieces
5 which were transferred to shaking culture⁵⁴ (**Fig. 4G**). Almost all *Pkd1*^{-/-} and *Pkd2*^{-/-} NPC-derived
6 nephron organoids formed cysts of different sizes, whereas no cysts were formed in *EGFP*^{-/-} con-
7 trol organoids (**Fig. 4H and I**). Cysts formed at similar efficiency following a freeze-and-thaw cycle,
8 opening up opportunities for easy transportation and distribution of ready-to-use PKD organoids
9 (**Fig. S5E-G**).

10 Treatment with CFTRinh172⁶¹, metformin^{62,63}, and AZ505^{64,65}, previously reported to have
11 cyst growth suppressing activities, decreased the percentage of organoids undergoing cyst for-
12 mation and cyst diameter within the organoids (**Fig. 4J, S5H and I**). As expected, these PKD
13 organoids did not respond to tolvaptan, which is specific for cystic cells of ureteric progenitor cell-
14 derived collecting duct epithelium^{66,67}. Next, to establish a scalable PKD organoid model, we used
15 commercially available AggreWell plates to mass produce mini 3D NPC aggregates (1700 NPCs
16 per mini aggregate, making ~1500 mini aggregates in each well of a 6-well plate). After aggrega-
17 tion, the mini NPC aggregates were transferred into shaking culture, the setting for nephron in-
18 duction and cyst formation (**Fig. 4K and L**).

19 Under the optimized culture condition (**Fig. S6A-D, and Methods**), *Pkd1*^{-/-} or *Pkd2*^{-/-} NPC
20 aggregates differentiated into cystic nephron organoids under shaking culture in a synchronized
21 manner with the budding of cysts as early as 4 days after shaking culture (**Fig. S5J**). This method
22 allows a more rapid cystic organoid generation than current PKD organoids starting from hPSCs,
23 which require at least 3 weeks to form cysts⁵⁴⁻⁵⁸. In our system, the cysts continued to grow in
24 size over the next few days, at which point 100% of the observed mini nephron organoids formed
25 cysts with similar diameters (**Fig. 4M-O**). Thus, a rapid, efficient, and scalable organoid model for
26 PKD is established directly from genetically modified NPCs.

1
2 **A drug screen identifies PTC-209 as a potential drug candidate for PKD treatment.**
3 We further determined whether the NPC-derived PKD organoids recapitulates key molecular, cel-
4 lular, and metabolic features of PKD. Whole-mount immunostaining of the *Pkd2*^{-/-} cystic organoids
5 clearly showed the co-expression of LTL and CDH1 in the majority of the cyst-lining cells (**Fig.**
6 **5A**). Phosphorylated histone H3 (pHH3) staining indicated a dramatic elevation of proliferative
7 cells in the cyst-lining epithelial cells of the *Pkd2*^{-/-} organoids, as compared to the epithelial cells
8 in the control organoids (**Fig. 5A and B**). Consistently, starting from the same number of NPCs,
9 *Pkd2* knockout cystic organoids have significantly higher total genomic DNA (**Fig. S7A**), suggest-
10 ing increased cellular proliferation. At the molecular level, gene expression analysis clearly
11 showed enhanced expression of a group of cell cycle genes that promote cell proliferation in the
12 *Pkd2*^{-/-} organoid as compared to *GFP*^{-/-} organoids (**Fig. 5C**), and mTOR pathway^{68,69} and MYC^{70,71}
13 activity were significantly activated in these cystic organoids (**Fig. 5D and E**). Comparison of gene
14 expression in the cystic and non-cystic portions from the *Pkd2*^{-/-} organoids further confirmed that
15 it is the cystic portions contributed to the dramatic gene expression changes (**Fig. S7B-E**).

16 We then interrogated the metabolic status of the *Pkd2*^{-/-} organoids and the *GFP*^{-/-} organ-
17 oids using SeahorseXFp™ analysis. Both the oxygen consumption rate (OCR, indicator of oxida-
18 tive phosphorylation) and the extracellular acidification rate (ECAR, indicator of glycolysis) were
19 dramatically higher in the *Pkd2*^{-/-} organoids as compared to control organoids (**Fig. 5F, S7F-I, N,**
20 **and P**), consistent with the observed metabolic reprogramming in PKD in which the cyst-lining
21 cells use significantly more energy from glycolysis to support the high metabolic needs for cyst
22 growth^{72,73}. No further OCR and ECAR increases were observed in the *Pkd2*^{-/-} organoids upon
23 Oligomycin/FCCP treatment to metabolically stress the organoids, suggesting that cystic cells in
24 PKD organoid culture engaged maximal energy consumption in support of rapid growth (**Fig. 5F,**
25 **S7F-I, N, and P**). This is in contrast to the control *GFP*^{-/-} organoids, which showed a capacity to

1 increase energy consumption through both OCR and ECAR by 50-100% from baseline in re-
2 sponse to stress (**Fig. S7N**). Importantly, comparing undifferentiated NPCs with organoids indi-
3 cated the metabolic phenotypes following *Pkd2* removal were specific to differentiated epithelial
4 cells but not progenitor cells (**Fig. 5G, S7J-M, O, and P**). Moreover, although the oxidative (OCR)
5 to glycolytic (ECAR) metabolism ratio was unchanged in *Pkd2*^{-/-} NPCs relative to *GFP*^{-/-} NPCs,
6 the OCR/ECAR ratio was significantly elevated in control *GFP*^{-/-} organoids relative to that in *Pkd2*
7 ^{-/-} organoids (**Fig. S7P**). Thus, *Pkd2*^{-/-} organoids had reduced oxidative relative to glycolytic capac-
8 ity, which is consistent with prior reports demonstrating impaired mitochondrial oxidative function
9 in ADPKD cells and tissues lacking polycystin function^{74,75}. Taken together, the cultured NPC-
10 derived PKD organoid models recapitulate important molecular, cellular, and metabolic features
11 of ADPKD pathogenesis. Lastly, as proof-of-concept, we established a similar PKD organoid
12 model from a wild-type NPC line without endogenous CAS9 (**Fig. S8A-E**), opening new avenues
13 for modeling PKD from existing transgenic mouse strains that are of interest to PKD researchers.

14 We next set out to perform a proof-of-concept drug screen using our scalable PKD organ-
15 oid model described above (**Fig. 4K**). For our candidate pool, we selected a commercially avail-
16 able 148 small molecule library, which targets major pathways of the epigenome (**Fig. S8F and**
17 **Methods**). *Pkd2*^{-/-} NPC clones #4 and #5 were used as two biological replicates for the screen.
18 To allow robust statistical analyses, 30–50 mini organoids were seeded into each well of a 12-
19 well plate and cultured in suspension with shaking. Three days after nephron induction, small
20 molecules were added individually into the culture medium. Two days after drug treatment, sig-
21 nificant differences in cyst formation were observed, so we quantified the cyst forming efficiencies
22 and the cyst diameters (**Fig. 5H**). Out of the 148 small molecules, 14 showed significant inhibitory
23 effects on cyst formation in at least one biological replicate (**Fig. 5H and I**). As a positive control,
24 metfomin dose-dependently inhibited cyst formation while tolvaptan, a negative control, had no
25 effect (**Fig. S8G**). 12 of the 14 hits identified were shared between the two biological replicates

1 (Fig. 5I), among which 8 were HDAC inhibitors, and 3 were BRD4 inhibitors, two previously de-
2 scribed treatments for ADPKD^{76,77}. The other shared hit identified was PTC-209, a specific inhib-
3 itor of BMI-1, which has not been previously reported in ADPKD. PTC-209 emerged as a top hit
4 for cyst inhibiting properties in the screen (Fig. 5J-L). Secondary validation further confirmed that
5 it can decrease cyst forming efficiency and cyst diameters in a dose-dependent manner (Fig.
6 S8H-J). Taken together, a proof-of-concept drug screen was performed, leading to the discovery
7 of a prospective drug candidate, PTC-209, for ADPKD treatment.

8

9 **YAP activation captures human NPCs with restored distal nephron differentiation potential.**
10 The broad applications of mouse NPC lines in 2D culture format inspired us to determine whether
11 we can also derive long-term expandable human NPC lines in 2D. For that, we first performed
12 immunostaining in human fetal kidney sections and verified that p38 MAPK activity (phosphory-
13 lated p38, p-p38, Fig. 6B), TGF- β signaling (phosphorylated Smad2/3, p-Smad2/3, Fig. 6C) and
14 BMP signaling (phosphorylated Smad1/5/8, p-Smad1/5/8, Fig. 6D), are intrinsically inhibited in
15 the primary hNPCs *in vivo*. Thus, we included p38, TGF- β , and BMP inhibitors in the culture
16 medium to expand human NPCs as we did in mNPSR-v2. By replacing mouse LIF with human
17 LIF in the mNPSR-v2 medium (mouse LIF does not activate human LIF receptors), we prepared
18 a culture medium, designated as hNPSR-v1, to determine whether it was suitable for 2D expan-
19 sion of human NPCs. For that, we first engineered H1 human embryonic stem cells (hESCs) with
20 CRISPR-Cas9 to knock in a dual reporter system for *SIX2*-GFP and *PAX2*-mCherry. Following a
21 well-established 10-day hPSC-to-NPC differentiation protocol⁸ (Fig. S9A), the *SIX2*⁺/*PAX2*⁺ in-
22 duced NPC (iNPC) population was collected by FACS (Fig. S9B) and cultured in hNPSR-v1 me-
23 dium. However, iNPCs were only able to stably expand for the first 2 weeks before cell prolifera-
24 tion slowed down with decreased NPC marker gene expression (data not shown), suggesting
25 hNPSR-v1 medium was not optimal for long-term expansion of iNPCs.

1 iNPCs cultured in hNPSR-v1 medium frequently lost YAP expression in the nucleus, sug-
2 gesting spontaneous loss of YAP activity (**Fig. 6E**). Considering the established role of YAP ac-
3 tivity in the self-renewal of various types of stem cells and progenitor cells^{78,79}, including NPCs⁸⁰,
4 we supplemented hNPSR-v1 medium with our recently reported, highly specific small molecule
5 YAP agonist TRULI⁸¹. Addition of 2 μ M to 4 μ M TRULI to an hNPSR-v2 formulation (**Table S12**),
6 resulted in significant nuclear accumulation of YAP in most iNPC nuclei (**Fig. 6E and F**) and long-
7 term clonal 2D expansion of iNPCs (**Fig. 6 and S9**), and primary human NPCs (**Fig. S10**) for
8 several months with high purity.

9 iNPCs cultured in hNPSR-v2 grew quickly with a typical passaging ratio of 1:10 every 3–
10 4 days (**Fig. 6G and H**). After 3 weeks of culture, more than 95% of cells maintained expression
11 of SIX2/PAX2/WT1/SALL1/ITGA8 (**Fig. 6I and J**). After long-term culture of more than 3 months,
12 all the NPC marker genes were still retained, except for a gradual decrease of *PAX2* starting after
13 1 month of culture (**Fig. S9C-E**). iNPCs showed a clonal efficiency of 58-70% in reseeding exper-
14 iments (**Figs. 6K and L, S9F and G**). Importantly, the robustness of hNPSR-v2 allowed us to
15 derive iNPC lines without prior FACS enrichment of the SIX2⁺/PAX2⁺ iNPCs (**Fig. 6A, S9H-J and**
16 **Methods**), suggesting iNPC lines might be derived from any hPSC lines, which greatly broadens
17 this application. Further, primary human NPCs were stably expanded in hNPSR-v2 medium for
18 100 days with the retention of NPC marker gene expression (**Fig. S10A-J**).

19 To compare their transcriptomes, bulk RNA-seq transcriptional profiling was performed on
20 iNPCs FACS sorted 10 days after initiation of hPSC differentiation without further culture, and
21 cultured human NPCs (day 15 to day 80) from different sources (iNPC or primary NPC) (**Table**
22 **S13**). Their transcriptional profiles were compared to recently published bulk RNA-seq data for
23 primary human NPCs freshly isolated from the human fetal kidney²⁴. Unsupervised PCA analysis
24 clustered the samples into 5 groups: “SIX2⁻ primary non-NPCs” (SIX2⁻ cells from human fetal
25 kidney²⁴); “SIX2⁺ primary NPCs”, “iNPCs with no culture;” “cultured NPCs in v1 medium;” and
26 “cultured NPCs in v2 medium” (**Fig. 6M, N, and S9K**). As expected, the “SIX2⁻ primary non-NPCs”

1 were positioned far from the other NPC groups along the PC1 axis. Interestingly, compared to
2 iNPCs without further culture, or cultured in the v1 medium, NPCs cultured in the v2 medium were
3 closer to the primary NPC state, which largely overlapped with the “SIX2⁺ primary NPCs” in both
4 PC1 and PC3 axes (**Fig. 6M and N**). Consistent with PCA, heatmap of gene expression of NPC
5 marker genes and nephron segment anchor genes also clustered the cultured NPCs closer to the
6 primary NPCs than iNPCs without any culture (**Fig. 6O**). Expression of nephron segment anchor
7 genes was not observed in any NPC group. However, compared to primary NPCs and cultured
8 NPCs, iNPCs without further culture showed significantly lower expression of *SIX2*, *HOXA11*, and
9 *HOXD11* genes, which encode transcription factors essential for NPC identity, suggesting that
10 following 10 days of directed differentiation from hPSCs, the iNPCs might still not be sufficiently
11 programmed to the NPC state, but after further culture, they transition to a state similar to the
12 primary NPCs. Furthermore, we showed that genetic manipulations, including lentiviral gene over-
13 expression and CRISPR-Cas9 based gene knock-in, can be efficiently conducted in the cultured
14 iNPCs, opening new avenues of applications for this system (**Fig. 6P and Q**).

15 To further validate the nephrogenic potential of the cultured NPCs, we generated nephron
16 organoids from the cultured NPCs, following a protocol that involves a pulse of Wnt activation
17 followed by spontaneous self-organization (**Fig. S10K, and Methods**). Mimicking normal nephro-
18 genesis, clear mesenchymal-to-epithelial transition was observed in the organoid in the first 3
19 days after Wnt activation, eventually forming numerous renal tubule-like structures with *PAX2*-
20 mCherry reporter expression over a course of 14 days (**Fig. S9L**). Immunostaining further con-
21 firmed the formation of various nephron segments, including *PODXL*⁺ glomeruli, *LTL*⁺/*HNF4A*⁺
22 proximal tubule, and *PAX2*⁺/*SLC12A1*⁺ loop of Henle (**Fig. 6R and S**). Interestingly, we observed
23 the formation of large numbers of *SLC12A3*⁺ distal convoluted tubule structures (**Fig. 6T and U**),
24 which are not detected in currently available human kidney organoids^{14,15,82-84}. Interestingly,
25 iNPCs cultured for a short period of time of 4 days generated significantly fewer *SLC12A3*⁺ distal
26 tubule structures compared to the iNPCs cultured for 32 days or 42 days (**Fig. 6T and U**). Similarly,

1 significantly more AQP1⁺ thin descending limbs of loop of Henle and LRP2⁺ proximal tubules were
2 generated from the long-term cultured iNPCs (**Fig. 6T**), and functional transporters SLC27A2 and
3 SLC34A1 found in the proximal tubule were expressed only from the long-term cultured iNPC-
4 derived organoids (**Fig. 6U and S9M**). Other genes that represent kidney terminal differentiation,
5 such as *SLC22A8*, *SPTSSB*, and *UMOD*, were also expressed at higher levels in the organoids
6 derived from iNPCs cultured long-term rather than short-term (**Fig. S9P**). Based on these obser-
7 vations, and the previous transcriptome analyses, we hypothesized that, upon further culture in
8 hNPSR-v2 medium, hPSC-derived iNPCs are programmed to a state closer to the native NPC
9 state, eventually gaining the more complete nephrogenic potential of generating all major seg-
10 ments of the human nephron, including the distal convoluted tubules.

11 Current kidney organoids generate a significant amount of off-target cell populations such
12 as neurons and myocytes^{14,15,82,83}. In contrast, in the cultured iNPC-derived nephron organoids,
13 MAP2 and NeuN, two neuron genes frequently expressed in current kidney organoids, were not
14 detected (**Fig. S9N and O**), reflecting the high purity of the cultured NPCs, and the restricted
15 developmental potential of NPCs only to the nephron. Similar results were observed in the neph-
16 ron organoids that were derived from long-term cultured primary human NPCs (**Fig. S10L-N**).
17

18 **Rapid, efficient, and scalable PKD modeling directly from genome-edited human NPCs.**
19 Based on the robust 2D culture system for long-term expansion of human NPCs, we de-
20 veloped a rapid, efficient, and scalable PKD organoid model directly from genome-edited
21 human NPCs (**Fig. 7A**). The *PKD2* gene was knocked out using CRISPR/Cas9 system
22 in our *SIX2*-GFP reporter hPSC line. Two single cell clones, #10 and #11, with verified
23 biallelic frame-shift mutations (**Fig. 7B-D**), were selected to derive NPC lines in hNPSR-
24 v2 medium. Mini NPC aggregates were generated, followed by shaking culture and neph-
25 ron induction (**Fig. 7A, E and Methods**). After 8 days of shaking culture, cysts emerged

1 in the *PKD2*^{-/-} NPC-derived nephron organoids, but not in the wild-type NPC-derived con-
2 trol organoids. These cysts continued to grow larger with the majority of the cyst-lining
3 cells expressing LTL and CDH1 (**Fig. 7F-I**). We then verified the responses of these cystic
4 organoids to previously described candidate PKD drug treatments. As expected,
5 CFTRinh172, metformin, AZ505, tubacin⁸⁵, and our newly identified small molecule PTC-
6 209, significantly decreased cyst forming efficiencies and cyst diameters, but not tolvaptan
7 (**Fig. 7J-L**). Thus, as proof-of-concept, with this scalable mini PKD organoid model, start-
8 ing from the expandable *PKD2*^{-/-} NPCs, a drug candidate's effects on cyst development
9 can be quantitatively determined within 8 days of shaking culture, which is a remarkably
10 faster turnaround than current PKD organoid models starting from hPSCs that require at
11 least 3 weeks⁵⁴⁻⁵⁸.

12

13 **DISCUSSION**

14 NPCs play central roles in kidney development and disease and have great potential in kidney
15 regenerative medicine. In this study, we redefine the critical role of p38 and YAP activity in NPC
16 self-renewal. Based on p38 inhibition and YAP activation, we developed chemically-defined cul-
17 ture systems for the clonal, long-term expansion of near pure mouse and human NPCs in 2D
18 culture. The culture system constitutes a synthetic niche that recapitulates developing nephron's
19 plasticity. Cultured NPCs show gene expression profiles similar to primary NPCs and generate
20 major segments of the nephron, including distal convoluted tubules, on differentiation in culture.
21 Genome-wide CRISPR screen of cultured NPCs demonstrated the potential of the model for ge-
22 nome-scale study of NPC biology, Wilms tumor, and CAKUT. Further, a rapid, efficient, and scal-
23 able PKD organoid model initiated from genome-edited NPCs, highlighted the potential for *de*
24 *novo* drug identification or validation. We anticipate that, with the simplicity and the robustness of

1 the protocols, these NPC and organoid culture systems will be widely adopted by other research-
2 ers to study different aspects of kidney development, disease, plasticity, and regeneration.

3 The inhibition of p38 MAPK activity proved to be key in allowing the long-term expansion
4 of mouse and human NPCs *in vitro* in the 2D culture setting. How p38 activity and its downstream
5 regulatory network control NPC self-renewal and differentiation remains to be determined. Simi-
6 larly, how activation of YAP signaling programs hPSC-derived iNPCs to a state similar to the
7 primary NPCs and then stably maintaining this state in culture also remains obscure. Our *in vitro*
8 accessible NPC culture systems will provide an ideal platform to address these important biolog-
9 ical questions.

10 As observed *in vivo*²⁵, we showed that *Wnt4*⁺ nephron cells have developmental plasticity
11 to be reprogrammed back to the NPC state *in vitro* in the NPC culture medium. Of note, *Wnt4*⁺
12 cells might not be the only plastic cell type in the developing kidney that can be reprogrammed to
13 the NPC state. For example, *Foxd1*⁺ IPCs and NPCs are believed to be derived from the same
14 precursor cells during early kidney development, with interchangeable cell identity^{86,87}. Thus, it is
15 conceivable that IPCs might also be readily reprogrammed to the NPC state. It will also be im-
16 portant to determine whether similar plasticity exists in the human kidney in the future. If so, the
17 mechanisms might be employed to develop *in vivo* reprogramming strategies for kidney regener-
18 ation and disease intervention.

19 Our observation that hPSC-derived iNPCs are not fully programmed to the NPC stage in
20 existing kidney organoids agrees with a recent report where an improvement in NPC specification
21 in organoid culture led to normalized proximal tubule specification and function though distal con-
22 voluted tubule cells were absent from organoids in this study¹⁶. As the currently only available
23 human kidney organoid system to generate abundant distal convoluted tubules, our platform will
24 open new avenues to study how human distal nephron fate is specified from NPCs, and allow
25 modeling of diseases that affect the distal nephron of the kidney.

1 PTC-209 was identified initially as a specific inhibitor of BMI-1, a gene that plays critical
2 roles in the self-renewal of stem cells in normal tissues and cancer⁸⁸. PTC-209 and its derivatives
3 are being tested in preclinical and clinical trials for the treatment of several types of cancer^{88,89}.
4 Considering that there are similarities between PKD and cancer pathogenesis⁹⁰, and given the
5 efficacy of PTC-209 in cyst inhibition in our organoid model, we propose that PTC-209 or other
6 BMI-1 inhibitors might be prospective candidates for PKD treatment. Future investigations using
7 animal models are warranted for BMI-1 inhibitors. In addition to PKD, we anticipate other kidney
8 disease models can also be established from kidney organoids derived directly from genome-
9 edited NPCs.

10

11 **Limitations of the study**

12 Like all other cell culture systems, cultured cells *in vitro* can recapitulate key features of their
13 counterparts *in vivo*, but may also gain characteristics that reflect *in vitro* culture. These differ-
14 ences usually do not prevent the broad applications of the *in vitro* cultured cells. However, when
15 interpreting the CRISPR screen results, we anticipate a small number of genes might be identified
16 as false positive hits due to differences based on *in vitro* culture. An example we observed is the
17 *Pax2* gene, encoding a transcription factor well-known for maintaining NPC identity^{87,91}. It was
18 expected to be negatively selected, considering that it is essential for NPC self-renewal, but in-
19 stead, it was identified as a top positively selected gene in the CRISPR screen. Thus, although
20 our CRISPR screen data provide a valuable list of genes that are functionally important *in vitro* in
21 NPC self-renewal, complementary approaches are still needed to validate the functions of specific
22 genes of interest *in vivo*, as in all other CRISPR screen studies.

23

24 **ACKNOWLEDGEMENTS**

25 We would like to thank Jeffrey Boyd and Bernadette Masinsin of the USC Flow Cytometry Facility
26 for FACS, Seth Ruffins of the USC Optical Imaging Facility for help with microscopy, Dejerianne

1 Ostrow and David Ruble of the Children's Hospital Los Angeles Molecular Pathology Genomics
2 Core for RNA-seq, Yibu Chen of the USC Norris Medical Library Bioinformatics Service for help
3 with the RNA-seq computational analysis, Dr. Melissa L. Wilson (Department of Preventive Med-
4 icine, University of Southern California) and Family Planning Associates for coordinating fetal
5 tissue collection, and Cristy Lytal for help with editing the manuscript. This work was supported
6 by UKRO foundation funding, a KSOM Dean's Pilot Award and an NIH Director's New Innovator
7 Award (DP2DK135739) to Z.L., and NIH DK054364 to A.P.M. Z.Z. was supported by a USC Stem
8 Cell Challenge Award. M.E.S. was supported by a CIRM Bridges Award.

9

10 **AUTHOR CONTRIBUTIONS**

11 Conceptualization, B.H. and Z.L.; methodology, investigation and validation, B.H., Z.Z., H.L., X.C.,
12 J.G., C.C.Z., M.E.S., A.C.V., T.X., T.P., Y.L., R.K.P., B.D., and J.H.C.; software and formal anal-
13 ysis, B.H., Z.Z., Z.L., and T.F.; resources, M.E.T., B.H.G., Y.D., Y.D., Q.Y., K.G., N.O.L., and
14 A.P.M.; writing – original draft, B.H. and Z.Z.; writing – review and editing, T.F., N.M.P.S., K.R.H.,
15 A.P.M. and Z.L.

16

17 **DECLARATION OF INTERESTS**

18 A.P.M. is a scientific advisor or consultant for Novartis, eGENESIS, Trestle Biotherapeutics and
19 IVIVA Medical. All other authors declare no competing interests.

20

21 **REFERENCES:**

22

23 1 McMahon, A. P. Development of the Mammalian Kidney. *Curr Top Dev Biol* **117**, 31-64
24 (2016). <https://doi.org/10.1016/bs.ctdb.2015.10.010>

25 2 Schnell, J., Achieng, M. & Lindström, N. O. Principles of human and mouse nephron
26 development. *Nat Rev Nephrol* (2022). <https://doi.org/10.1038/s41581-022-00598-5>

27 3 Kobayashi, A. *et al.* Six2 defines and regulates a multipotent self-renewing nephron
28 progenitor population throughout mammalian kidney development. *Cell Stem Cell* **3**, 169-
29 181 (2008). <https://doi.org/10.1016/j.stem.2008.05.020>

1 4 van der Ven, A. T., Vivante, A. & Hildebrandt, F. Novel Insights into the Pathogenesis of
2 Monogenic Congenital Anomalies of the Kidney and Urinary Tract. *J Am Soc Nephrol* **29**,
3 36-50 (2018). <https://doi.org/10.1681/ASN.2017050561>

4 5 Treger, T. D., Chowdhury, T., Pritchard-Jones, K. & Behjati, S. The genetic changes of
5 Wilms tumour. *Nat Rev Nephrol* **15**, 240-251 (2019). <https://doi.org/10.1038/s41581-019-0112-0>

6 Taguchi, A. *et al.* Redefining the in vivo origin of metanephric nephron progenitors
7 enables generation of complex kidney structures from pluripotent stem cells. *Cell Stem
8 Cell* **14**, 53-67 (2014). <https://doi.org/10.1016/j.stem.2013.11.010>

9 Freedman, B. S. *et al.* Modelling kidney disease with CRISPR-mutant kidney organoids
10 derived from human pluripotent epiblast spheroids. *Nat Commun* **6**, 8715 (2015).
11 <https://doi.org/10.1038/ncomms9715>

12 Morizane, R. *et al.* Nephron organoids derived from human pluripotent stem cells model
13 kidney development and injury. *Nat Biotechnol* **33**, 1193-1200 (2015).
14 <https://doi.org/10.1038/nbt.3392>

15 Takasato, M. *et al.* Kidney organoids from human iPS cells contain multiple lineages and
16 model human nephrogenesis. *Nature* **526**, 564-568 (2015).
17 <https://doi.org/10.1038/nature15695>

18 Brown, A. C., Muthukrishnan, S. D. & Oxburgh, L. A synthetic niche for nephron progenitor
19 cells. *Dev Cell* **34**, 229-241 (2015). <https://doi.org/10.1016/j.devcel.2015.06.021>

20 Tanigawa, S., Taguchi, A., Sharma, N., Perantoni, A. O. & Nishinakamura, R. Selective
21 In Vitro Propagation of Nephron Progenitors Derived from Embryos and Pluripotent Stem
22 Cells. *Cell Rep* **15**, 801-813 (2016). <https://doi.org/10.1016/j.celrep.2016.03.076>

23 Li, Z. *et al.* 3D Culture Supports Long-Term Expansion of Mouse and Human Nephrogenic
24 Progenitors. *Cell Stem Cell* **19**, 516-529 (2016).
25 <https://doi.org/10.1016/j.stem.2016.07.016>

26 Little, M. H. & Combes, A. N. Kidney organoids: accurate models or fortunate accidents.
27 *Genes Dev* **33**, 1319-1345 (2019). <https://doi.org/10.1101/gad.329573.119>

28 Wu, H. *et al.* Comparative Analysis and Refinement of Human PSC-Derived Kidney
29 Organoid Differentiation with Single-Cell Transcriptomics. *Cell Stem Cell* **23**, 869-881.e868
30 (2018). <https://doi.org/10.1016/j.stem.2018.10.010>

31 Combes, A. N., Zappia, L., Er, P. X., Oshlack, A. & Little, M. H. Single-cell analysis reveals
32 congruence between kidney organoids and human fetal kidney. *Genome Med* **11**, 3 (2019).
33 <https://doi.org/10.1186/s13073-019-0615-0>

34 Vanslambrouck, J. M. *et al.* Enhanced metanephric specification to functional proximal
35 tubule enables toxicity screening and infectious disease modelling in kidney organoids.
36 *Nat Commun* **13**, 5943 (2022). <https://doi.org/10.1038/s41467-022-33623-z>

37 Shalem, O. *et al.* Genome-scale CRISPR-Cas9 knockout screening in human cells. *Science*
38 **343**, 84-87 (2014). <https://doi.org/10.1126/science.1247005>

39 Wang, T., Wei, J. J., Sabatini, D. M. & Lander, E. S. Genetic screens in human cells using
40 the CRISPR-Cas9 system. *Science* **343**, 80-84 (2014).
41 <https://doi.org/10.1126/science.1246981>

42 Doench, J. G. Am I ready for CRISPR? A user's guide to genetic screens. *Nat Rev Genet* **19**,
43 67-80 (2018). <https://doi.org/10.1038/nrg.2017.97>

44

1 20 Tanigawa, S. *et al.* Activin Is Superior to BMP7 for Efficient Maintenance of Human iPSC-
2 Derived Nephron Progenitors. *Stem Cell Reports* **13**, 322-337 (2019).
3 <https://doi.org/10.1016/j.stemcr.2019.07.003>

4 21 Li, Z., Araoka, T. & Belmonte, J. C. I. Gene Editing in 3D Cultured Nephron Progenitor Cell
5 Lines. *Methods Mol Biol* **1926**, 151-159 (2019). https://doi.org/10.1007/978-1-4939-9021-4_13

6 22 Zeng, Z. *et al.* Generation of patterned kidney organoids that recapitulate the adult kidney
7 collecting duct system from expandable ureteric bud progenitors. *Nat Commun* **12**, 3641
8 (2021). <https://doi.org/10.1038/s41467-021-23911-5>

9 23 Garreta, E. *et al.* Fine tuning the extracellular environment accelerates the derivation of
10 kidney organoids from human pluripotent stem cells. *Nat Mater* **18**, 397-405 (2019).
11 <https://doi.org/10.1038/s41563-019-0287-6>

12 24 Lindström, N. O. *et al.* Conserved and Divergent Features of Mesenchymal Progenitor Cell
13 Types within the Cortical Nephrogenic Niche of the Human and Mouse Kidney. *J Am Soc
14 Nephrol* **29**, 806-824 (2018). <https://doi.org/10.1681/ASN.2017080890>

15 25 Lawlor, K. T. *et al.* Nephron progenitor commitment is a stochastic process influenced by
16 cell migration. *Elife* **8** (2019). <https://doi.org/10.7554/elife.41156>

17 26 Przybyla, L. & Gilbert, L. A. A new era in functional genomics screens. *Nat Rev Genet* **23**,
18 89-103 (2022). <https://doi.org/10.1038/s41576-021-00409-w>

19 27 Doench, J. G. *et al.* Optimized sgRNA design to maximize activity and minimize off-target
20 effects of CRISPR-Cas9. *Nat Biotechnol* **34**, 184-191 (2016).
21 <https://doi.org/10.1038/nbt.3437>

22 28 Li, W. *et al.* Quality control, modeling, and visualization of CRISPR screens with MAGeCK-
23 VISPR. *Genome Biol* **16**, 281 (2015). <https://doi.org/10.1186/s13059-015-0843-6>

24 29 Wang, B. *et al.* Integrative analysis of pooled CRISPR genetic screens using MAGeCKFlute.
25 *Nat Protoc* **14**, 756-780 (2019). <https://doi.org/10.1038/s41596-018-0113-7>

26 30 Makayes, Y. *et al.* Increasing mTORC1 Pathway Activity or Methionine Supplementation
27 during Pregnancy Reverses the Negative Effect of Maternal Malnutrition on the
28 Developing Kidney. *J Am Soc Nephrol* **32**, 1898-1912 (2021).
29 <https://doi.org/10.1681/ASN.2020091321>

30 31 Volovelsky, O. *et al.* Hamartin regulates cessation of mouse nephrogenesis independently
31 of Mtor. *Proc Natl Acad Sci U S A* **115**, 5998-6003 (2018).
32 <https://doi.org/10.1073/pnas.1712955115>

33 32 Marrone, A. K. *et al.* MicroRNA-17~92 is required for nephrogenesis and renal function. *J
34 Am Soc Nephrol* **25**, 1440-1452 (2014). <https://doi.org/10.1681/ASN.2013040390>

35 33 Ho, J. *et al.* The pro-apoptotic protein Bim is a microRNA target in kidney progenitors. *J
36 Am Soc Nephrol* **22**, 1053-1063 (2011). <https://doi.org/10.1681/ASN.2010080841>

37 34 Cargill, K. *et al.* Von Hippel-Lindau Acts as a Metabolic Switch Controlling Nephron
38 Progenitor Differentiation. *J Am Soc Nephrol* **30**, 1192-1205 (2019).
39 <https://doi.org/10.1681/ASN.2018111170>

40 35 Nishinakamura, R. *et al.* Murine homolog of SALL1 is essential for ureteric bud invasion in
41 kidney development. *Development* **128**, 3105-3115 (2001).

42

1 36 Kanda, S. *et al.* Sall1 maintains nephron progenitors and nascent nephrons by acting as
2 both an activator and a repressor. *J Am Soc Nephrol* **25**, 2584-2595 (2014).
3 <https://doi.org/10.1681/ASN.2013080896>

4 37 Basta, J. M., Robbins, L., Kiefer, S. M., Dorsett, D. & Rauchman, M. Sall1 balances self-
5 renewal and differentiation of renal progenitor cells. *Development* **141**, 1047-1058 (2014).
6 <https://doi.org/10.1242/dev.095851>

7 38 Motamedi, F. J. *et al.* WT1 controls antagonistic FGF and BMP-pSMAD pathways in early
8 renal progenitors. *Nat Commun* **5**, 4444 (2014). <https://doi.org/10.1038/ncomms5444>

9 39 Motojima, M., Tanaka, M. & Kume, T. Foxc1 and Foxc2 are indispensable for the
10 maintenance of nephron and stromal progenitors in the developing kidney. *J Cell Sci* **135**
11 (2022). <https://doi.org/10.1242/jcs.260356>

12 40 Pan, X., Karner, C. M. & Carroll, T. J. Myc cooperates with β -catenin to drive gene
13 expression in nephron progenitor cells. *Development* **144**, 4173-4182 (2017).
14 <https://doi.org/10.1242/dev.153700>

15 41 Xu, J. *et al.* Eya1 interacts with Six2 and Myc to regulate expansion of the nephron
16 progenitor pool during nephrogenesis. *Dev Cell* **31**, 434-447 (2014).
17 <https://doi.org/10.1016/j.devcel.2014.10.015>

18 42 Chen, Z. *et al.* Jxc1/Sobp, encoding a nuclear zinc finger protein, is critical for cochlear
19 growth, cell fate, and patterning of the organ of corti. *J Neurosci* **28**, 6633-6641 (2008).
20 <https://doi.org/10.1523/JNEUROSCI.1280-08.2008>

21 43 Tavares, A. L. P., Jourdeuil, K., Neilson, K. M., Majumdar, H. D. & Moody, S. A. Sobp
22 modulates the transcriptional activation of Six1 target genes and is required during
23 craniofacial development. *Development* **148** (2021). <https://doi.org/10.1242/dev.199684>

24 44 Atlasi, Y. & Stunnenberg, H. G. The interplay of epigenetic marks during stem cell
25 differentiation and development. *Nat Rev Genet* **18**, 643-658 (2017).
26 <https://doi.org/10.1038/nrg.2017.57>

27 45 Avgustinova, A. & Benitah, S. A. Epigenetic control of adult stem cell function. *Nat Rev
28 Mol Cell Biol* **17**, 643-658 (2016). <https://doi.org/10.1038/nrm.2016.76>

29 46 Huang, B., Liu, Z., Vonk, A., Zeng, Z. & Li, Z. Epigenetic regulation of kidney progenitor cells.
30 *Stem Cells Transl Med* **9**, 655-660 (2020). <https://doi.org/10.1002/sctm.19-0289>

31 47 Liu, H. *et al.* Histone deacetylases 1 and 2 regulate the transcriptional programs of
32 nephron progenitors and renal vesicles. *Development* **145** (2018).
33 <https://doi.org/10.1242/dev.153619>

34 48 Denner, D. R. & Rauchman, M. Mi-2/NuRD is required in renal progenitor cells during
35 embryonic kidney development. *Dev Biol* **375**, 105-116 (2013).
36 <https://doi.org/10.1016/j.ydbio.2012.11.018>

37 49 Liu, H. *et al.* The polycomb proteins EZH1 and EZH2 co-regulate chromatin accessibility
38 and nephron progenitor cell lifespan in mice. *J Biol Chem* **295**, 11542-11558 (2020).
39 <https://doi.org/10.1074/jbc.RA120.013348>

40 50 Basta, J. M. *et al.* The core SWI/SNF catalytic subunit Brg1 regulates nephron progenitor
41 cell proliferation and differentiation. *Dev Biol* **464**, 176-187 (2020).
42 <https://doi.org/10.1016/j.ydbio.2020.05.008>

1 51 van der Ven, A. T. *et al.* Whole-Exome Sequencing Identifies Causative Mutations in
2 Families with Congenital Anomalies of the Kidney and Urinary Tract. *J Am Soc Nephrol* **29**,
3 2348-2361 (2018). <https://doi.org/10.1681/ASN.2017121265>

4 52 Yu, X. *et al.* A selective WDR5 degrader inhibits acute myeloid leukemia in patient-derived
5 mouse models. *Sci Transl Med* **13**, eabj1578 (2021).
6 <https://doi.org/10.1126/scitranslmed.abj1578>

7 53 Bergmann, C. *et al.* Polycystic kidney disease. *Nat Rev Dis Primers* **4**, 50 (2018).
8 <https://doi.org/10.1038/s41572-018-0047-y>

9 54 Cruz, N. M. *et al.* Organoid cystogenesis reveals a critical role of microenvironment in
10 human polycystic kidney disease. *Nat Mater* **16**, 1112-1119 (2017).
11 <https://doi.org/10.1038/nmat4994>

12 55 Czerniecki, S. M. *et al.* High-Throughput Screening Enhances Kidney Organoid
13 Differentiation from Human Pluripotent Stem Cells and Enables Automated
14 Multidimensional Phenotyping. *Cell Stem Cell* **22**, 929-940.e924 (2018).
15 <https://doi.org/10.1016/j.stem.2018.04.022>

16 56 Kuraoka, S. *et al.* -Dependent Renal Cystogenesis in Human Induced Pluripotent Stem Cell-
17 Derived Ureteric Bud/Collecting Duct Organoids. *J Am Soc Nephrol* **31**, 2355-2371 (2020).
18 <https://doi.org/10.1681/ASN.2020030378>

19 57 Shimizu, T. *et al.* A novel ADPKD model using kidney organoids derived from disease-
20 specific human iPSCs. *Biochem Biophys Res Commun* **529**, 1186-1194 (2020).
21 <https://doi.org/10.1016/j.bbrc.2020.06.141>

22 58 Tran, T. *et al.* A scalable organoid model of human autosomal dominant polycystic kidney
23 disease for disease mechanism and drug discovery. *Cell Stem Cell* **29**, 1083-1101.e1087
24 (2022). <https://doi.org/10.1016/j.stem.2022.06.005>

25 59 Zuo, E. *et al.* One-step generation of complete gene knockout mice and monkeys by
26 CRISPR/Cas9-mediated gene editing with multiple sgRNAs. *Cell Res* **27**, 933-945 (2017).
27 <https://doi.org/10.1038/cr.2017.81>

28 60 Platt, R. J. *et al.* CRISPR-Cas9 knockin mice for genome editing and cancer modeling. *Cell*
29 **159**, 440-455 (2014). <https://doi.org/10.1016/j.cell.2014.09.014>

30 61 Yang, B., Sonawane, N. D., Zhao, D., Somlo, S. & Verkman, A. S. Small-molecule CFTR
31 inhibitors slow cyst growth in polycystic kidney disease. *J Am Soc Nephrol* **19**, 1300-1310
32 (2008). <https://doi.org/10.1681/ASN.2007070828>

33 62 Takiar, V. *et al.* Activating AMP-activated protein kinase (AMPK) slows renal cystogenesis.
34 *Proc Natl Acad Sci U S A* **108**, 2462-2467 (2011).
35 <https://doi.org/10.1073/pnas.1011498108>

36 63 Pastor-Soler, N. M. *et al.* Metformin improves relevant disease parameters in an
37 autosomal dominant polycystic kidney disease mouse model. *Am J Physiol Renal Physiol*
38 **322**, F27-F41 (2022). <https://doi.org/10.1152/ajprenal.00298.2021>

39 64 Li, L. X. *et al.* Lysine methyltransferase SMYD2 promotes cyst growth in autosomal
40 dominant polycystic kidney disease. *J Clin Invest* **127**, 2751-2764 (2017).
41 <https://doi.org/10.1172/JCI90921>

42 65 Li, L. X. *et al.* Cross talk between lysine methyltransferase Smyd2 and TGF- β -Smad3
43 signaling promotes renal fibrosis in autosomal dominant polycystic kidney disease. *Am J*

1 *Physiol Renal Physiol* **323**, F227-F242 (2022).
2 <https://doi.org/10.1152/ajprenal.00452.2021>

3 66 Torres, V. E. *et al.* Tolvaptan in patients with autosomal dominant polycystic kidney
4 disease. *N Engl J Med* **367**, 2407-2418 (2012). <https://doi.org/10.1056/NEJMoa1205511>
5 67 Reif, G. A. *et al.* Tolvaptan inhibits ERK-dependent cell proliferation, Cl⁻ secretion, and in
6 vitro cyst growth of human ADPKD cells stimulated by vasopressin. *Am J Physiol Renal
7 Physiol* **301**, F1005-1013 (2011). <https://doi.org/10.1152/ajprenal.00243.2011>
8 68 Shillingford, J. M. *et al.* The mTOR pathway is regulated by polycystin-1, and its inhibition
9 reverses renal cystogenesis in polycystic kidney disease. *Proc Natl Acad Sci U S A* **103**,
10 5466-5471 (2006). <https://doi.org/10.1073/pnas.0509694103>
11 69 Tao, Y., Kim, J., Schrier, R. W. & Edelstein, C. L. Rapamycin markedly slows disease
12 progression in a rat model of polycystic kidney disease. *J Am Soc Nephrol* **16**, 46-51 (2005).
13 <https://doi.org/10.1681/ASN.2004080660>
14 70 Cai, J. *et al.* A RhoA-YAP-c-Myc signaling axis promotes the development of polycystic
15 kidney disease. *Genes Dev* **32**, 781-793 (2018). <https://doi.org/10.1101/gad.315127.118>
16 71 Trudel, M., D'Agati, V. & Costantini, F. C-myc as an inducer of polycystic kidney disease in
17 transgenic mice. *Kidney Int* **39**, 665-671 (1991). <https://doi.org/10.1038/ki.1991.80>
18 72 Padovano, V., Podrini, C., Boletta, A. & Caplan, M. J. Metabolism and mitochondria in
19 polycystic kidney disease research and therapy. *Nat Rev Nephrol* **14**, 678-687 (2018).
20 <https://doi.org/10.1038/s41581-018-0051-1>
21 73 Rowe, I. *et al.* Defective glucose metabolism in polycystic kidney disease identifies a new
22 therapeutic strategy. *Nat Med* **19**, 488-493 (2013). <https://doi.org/10.1038/nm.3092>
23 74 Menezes, L. F., Lin, C. C., Zhou, F. & Germino, G. G. Fatty Acid Oxidation is Impaired in An
24 Orthologous Mouse Model of Autosomal Dominant Polycystic Kidney Disease.
25 *EBioMedicine* **5**, 183-192 (2016). <https://doi.org/10.1016/j.ebiom.2016.01.027>
26 75 Lin, C. C. *et al.* A cleavage product of Polycystin-1 is a mitochondrial matrix protein that
27 affects mitochondria morphology and function when heterologously expressed. *Sci Rep* **8**,
28 2743 (2018). <https://doi.org/10.1038/s41598-018-20856-6>
29 76 Cao, Y. *et al.* Chemical modifier screen identifies HDAC inhibitors as suppressors of PKD
30 models. *Proc Natl Acad Sci U S A* **106**, 21819-21824 (2009).
31 <https://doi.org/10.1073/pnas.0911987106>
32 77 Zhou, X. *et al.* Therapeutic targeting of BET bromodomain protein, Brd4, delays cyst
33 growth in ADPKD. *Hum Mol Genet* **24**, 3982-3993 (2015).
34 <https://doi.org/10.1093/hmg/ddv136>
35 78 Zanconato, F., Cordenonsi, M. & Piccolo, S. YAP/TAZ at the Roots of Cancer. *Cancer Cell*
36 **29**, 783-803 (2016). <https://doi.org/10.1016/j.ccr.2016.05.005>
37 79 Yu, F. X., Zhao, B. & Guan, K. L. Hippo Pathway in Organ Size Control, Tissue Homeostasis,
38 and Cancer. *Cell* **163**, 811-828 (2015). <https://doi.org/10.1016/j.cell.2015.10.044>
39 80 Das, A. *et al.* Stromal-epithelial crosstalk regulates kidney progenitor cell differentiation.
40 *Nat Cell Biol* **15**, 1035-1044 (2013). <https://doi.org/10.1038/ncb2828>
41 81 Kastan, N. *et al.* Small-molecule inhibition of Lats kinases may promote Yap-dependent
42 proliferation in postmitotic mammalian tissues. *Nat Commun* **12**, 3100 (2021).
43 <https://doi.org/10.1038/s41467-021-23395-3>

1 82 Subramanian, A. *et al.* Single cell census of human kidney organoids shows reproducibility
2 and diminished off-target cells after transplantation. *Nat Commun* **10**, 5462 (2019).
3 <https://doi.org/10.1038/s41467-019-13382-0>

4 83 Phipson, B. *et al.* Evaluation of variability in human kidney organoids. *Nat Methods* **16**,
5 79-87 (2019). <https://doi.org/10.1038/s41592-018-0253-2>

6 84 Tran, T. *et al.* In Vivo Developmental Trajectories of Human Podocyte Inform In Vitro
7 Differentiation of Pluripotent Stem Cell-Derived Podocytes. *Dev Cell* **50**, 102-116.e106
8 (2019). <https://doi.org/10.1016/j.devcel.2019.06.001>

9 85 Cebotaru, L. *et al.* Inhibition of histone deacetylase 6 activity reduces cyst growth in
10 polycystic kidney disease. *Kidney Int* **90**, 90-99 (2016).
11 <https://doi.org/10.1016/j.kint.2016.01.026>

12 86 Kobayashi, A. *et al.* Identification of a multipotent self-renewing stromal progenitor
13 population during mammalian kidney organogenesis. *Stem Cell Reports* **3**, 650-662 (2014).
14 <https://doi.org/10.1016/j.stemcr.2014.08.008>

15 87 Naiman, N. *et al.* Repression of Interstitial Identity in Nephron Progenitor Cells by Pax2
16 Establishes the Nephron-Interstitial Boundary during Kidney Development. *Dev Cell* **41**,
17 349-365.e343 (2017). <https://doi.org/10.1016/j.devcel.2017.04.022>

18 88 Kreso, A. *et al.* Self-renewal as a therapeutic target in human colorectal cancer. *Nat Med*
19 **20**, 29-36 (2014). <https://doi.org/10.1038/nm.3418>

20 89 Jia, L., Zhang, W. & Wang, C. Y. BMI1 Inhibition Eliminates Residual Cancer Stem Cells after
21 PD1 Blockade and Activates Antitumor Immunity to Prevent Metastasis and Relapse. *Cell*
22 *Stem Cell* **27**, 238-253.e236 (2020). <https://doi.org/10.1016/j.stem.2020.06.022>

23 90 Seeger-Nukpezah, T., Geynisman, D. M., Nikonova, A. S., Benzing, T. & Golemis, E. A. The
24 hallmarks of cancer: relevance to the pathogenesis of polycystic kidney disease. *Nat Rev*
25 *Nephrol* **11**, 515-534 (2015). <https://doi.org/10.1038/nrneph.2015.46>

26 91 Bouchard, M., Souabni, A., Mandler, M., Neubüser, A. & Busslinger, M. Nephric lineage
27 specification by Pax2 and Pax8. *Genes Dev* **16**, 2958-2970 (2002).
28 <https://doi.org/10.1101/gad.240102>

29

Figure 1

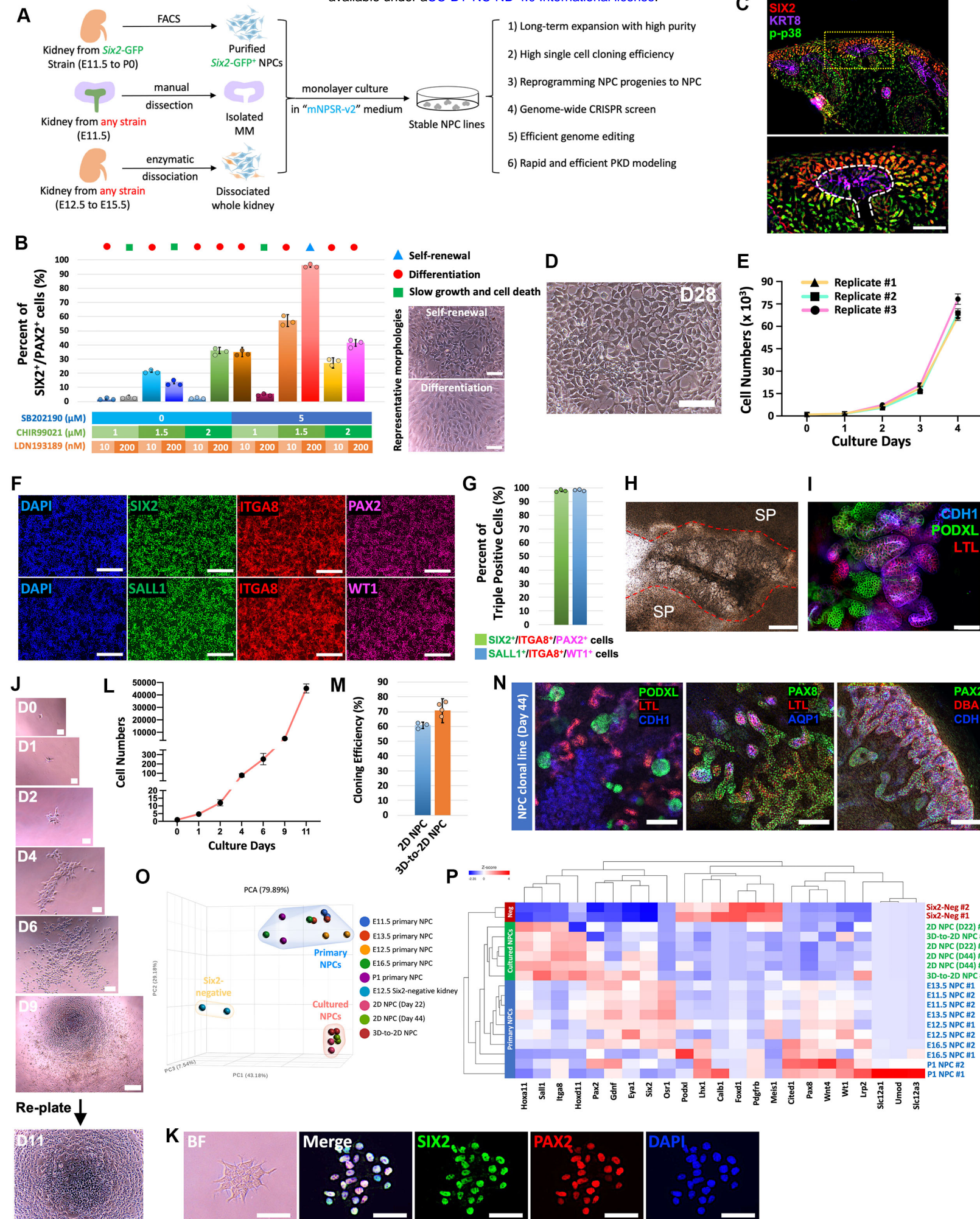


Figure 1. p38 inhibition allows the derivation of clonal expandable NPC lines from any mouse strain.

(A) Schematic of mNPC line derivation and the applications.

(B) Quantification of $SIX2^+$ / $PAX2^+$ cell percentages in mNPCs after 4 days of culture in media containing different concentrations of CHIR99021, LDN193189, and SB202190 as indicated, on top of mNPSR medium (left panel). Typical bright field images of self-renewing or differentiating mNPCs are shown on the right panels. Scale bars, 50 μ m.

(C) Immunostaining of E13.5 mouse kidney section for phosphorylated p38 (p-p38), NPC marker $SIX2$, and ureteric epithelium marker KRT8. Scale bar, 50 μ m.

(D) Morphology of mNPCs cultured in mNPSR-v2 medium for 28 days (D28). Scale bar, 50 μ m.

(E) Growth curve of mNPCs cultured in mNPSR-v2 medium in a typical passage cycle starting from 5,000 cells.

(F and G) Immunofluorescence staining (F) and quantification (G) of mNPCs cultured in mNPSR-v2 medium for 28 days for various NPC markers as indicated. Scale bars, 100 μ m.

(H) Bright-field image showing 7 days after co-culturing E12.5 spinal cord (SP) with aggregated mNPCs on Transwell filter. Red dashed lines indicate the boundaries between spinal cords and differentiated mNPCs. Scale bar, 200 μ m.

(I) Whole-mount immunofluorescence analysis of mNPC-derived nephron structures in (H) for marker genes representing different nephron segments. Scale bar, 100 μ m.

(J) Time-course bright-field images showing mNPC clonal expansion from one single cell. Scale bars, 50 μ m.

(K) Bright-field (BF) and immunofluorescence images of a representative single cell mNPC clone for NPC markers $SIX2$ and $PAX2$. Scale bars, 50 μ m.

(L) Growth curve of a single mNPC cultured in mNPSR-v2 medium over 11 days.

(M) Single cell cloning efficiency of mNPCs derived in 2D culture format (2D NPC), or transitioned from existing 3D-cultured mNPCs to 2D culture (3D-to-2D NPC).

(N) Whole-mount immunofluorescence analyses of nephron organoids generated from a clonal NPC line derived from parental mNPCs cultured in mNPSR-v2 for 44 days. Scale bars, 100 μ m.

(O) Three-dimensional presentation of principal component analysis (PCA) of bulk RNA-seq data of primary NPCs, NPCs cultured in mNPSR-v2 medium, and a negative control *Six2*-negative population from E12.5 kidney.

(P) Heatmap showing gene expression of selected marker genes for undifferentiated NPCs and differentiated kidney cell types, in primary and cultured NPCs, based on bulk RNA-seq datasets. Data are presented as mean \pm SD. Each column represents counts from three biological replicates (n=3).

See also Figure S1, S2 and Tables S1-S4.

Figure 2

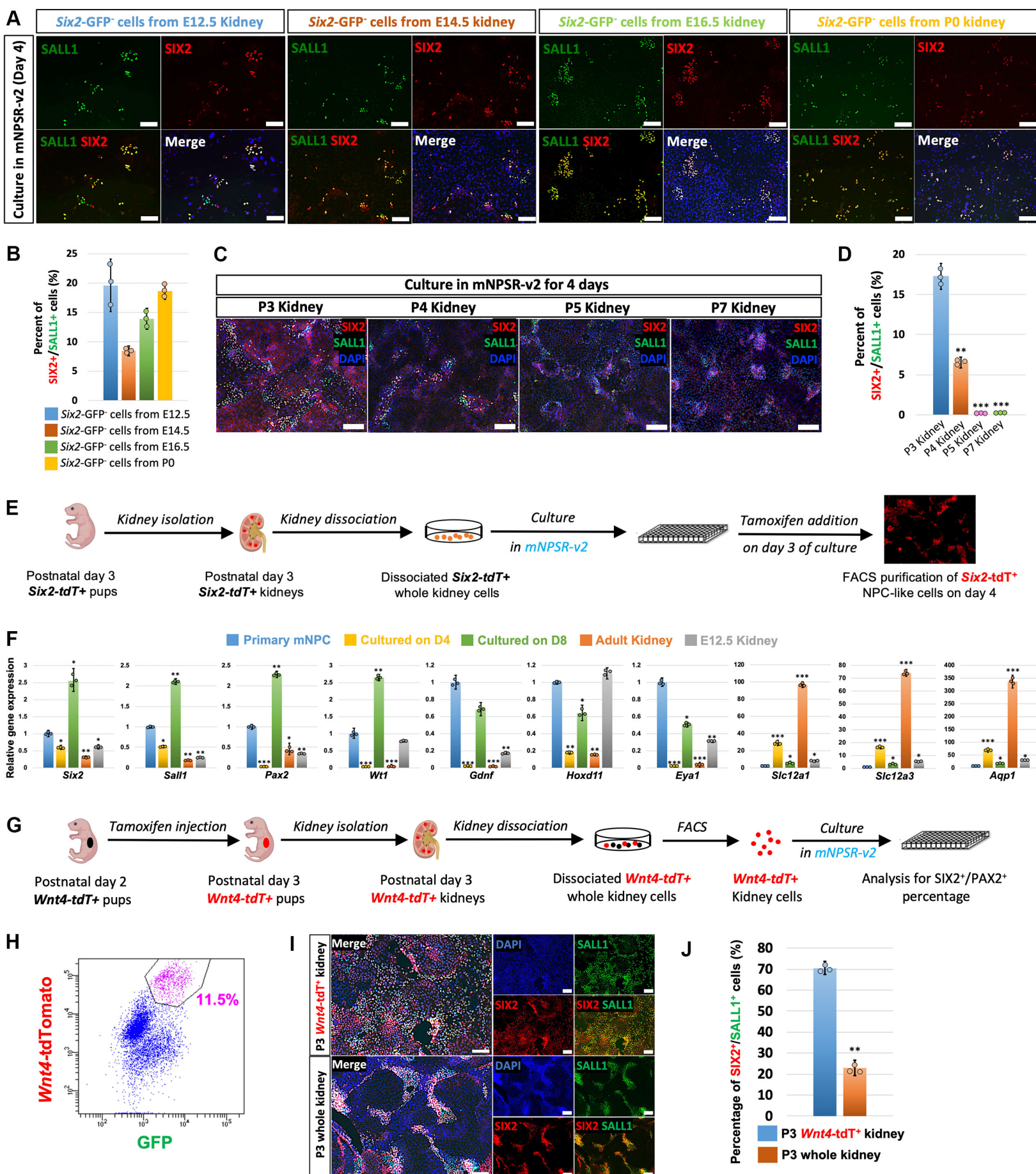


Figure 2. Capture the plasticity of developing nephron cells with mNPSR-v2 medium.

(A and B) Immunofluorescence images (A) and quantification (B) of the expression of NPC marker genes SIX2 and SALL1, in *Six2-GFP*⁺ cells isolated from E12.5, E14.5, E16.5, and P0 kidneys and cultured in mNPSR-v2 medium for 4 days. Scale bars, 100 μ m.

(C and D) Immunofluorescence images (C) and quantification (D) of the expression of SIX2 and SALL1 in P3, P4, P5, and P7 whole kidney cells cultured in mNPSR-v2 medium for 4 days. Note that only fluorescence signals in the nucleus were true SIX2 signals. Membrane-bound signals were from the non-specific binding of the SIX2 primary antibody. Scale bars, 100 μ m.

(E) Schematic showing the genetic labeling and FACS isolation of the induced *Six2-tdT*⁺ cells from P3 kidney cells cultured in mNPSR-v2 for 4 days.

(F) qRT-PCR analysis of primary mNPC, *Six2-tdT*⁺ cells cultured for 4 days and 8 days, adult kidney, and E12.5 kidney, for various marker genes of NPC and differentiated nephron cell types.

(G) Schematic showing the genetic labeling, FACS isolation, and culturing of *Wnt4-tdT*⁺ cells from P3 kidneys with mNPSR-v2 medium.

(H) Flow cytometry gating plot showing the purification of *Wnt4-tdT*⁺ cells from P3 kidneys.

(I and J) Immunofluorescence images (I) and quantification (J) of the expression of SIX2 and SALL1 in *Wnt4-tdT*⁺ kidney cells isolated from P3 kidney, and in whole P3 kidney cells, cultured in mNPSR-v2 medium for 4 days. Scale bars, 100 μ m.

Data are presented as mean \pm SD. Each column represents counts from three biological replicates (n=3). The significance was determined by two-tailed unpaired Student's t tests; ns, not significant; *, p<0.05; **, p<0.01; ***, p<0.001.

See also Figure S3.

Figure 3

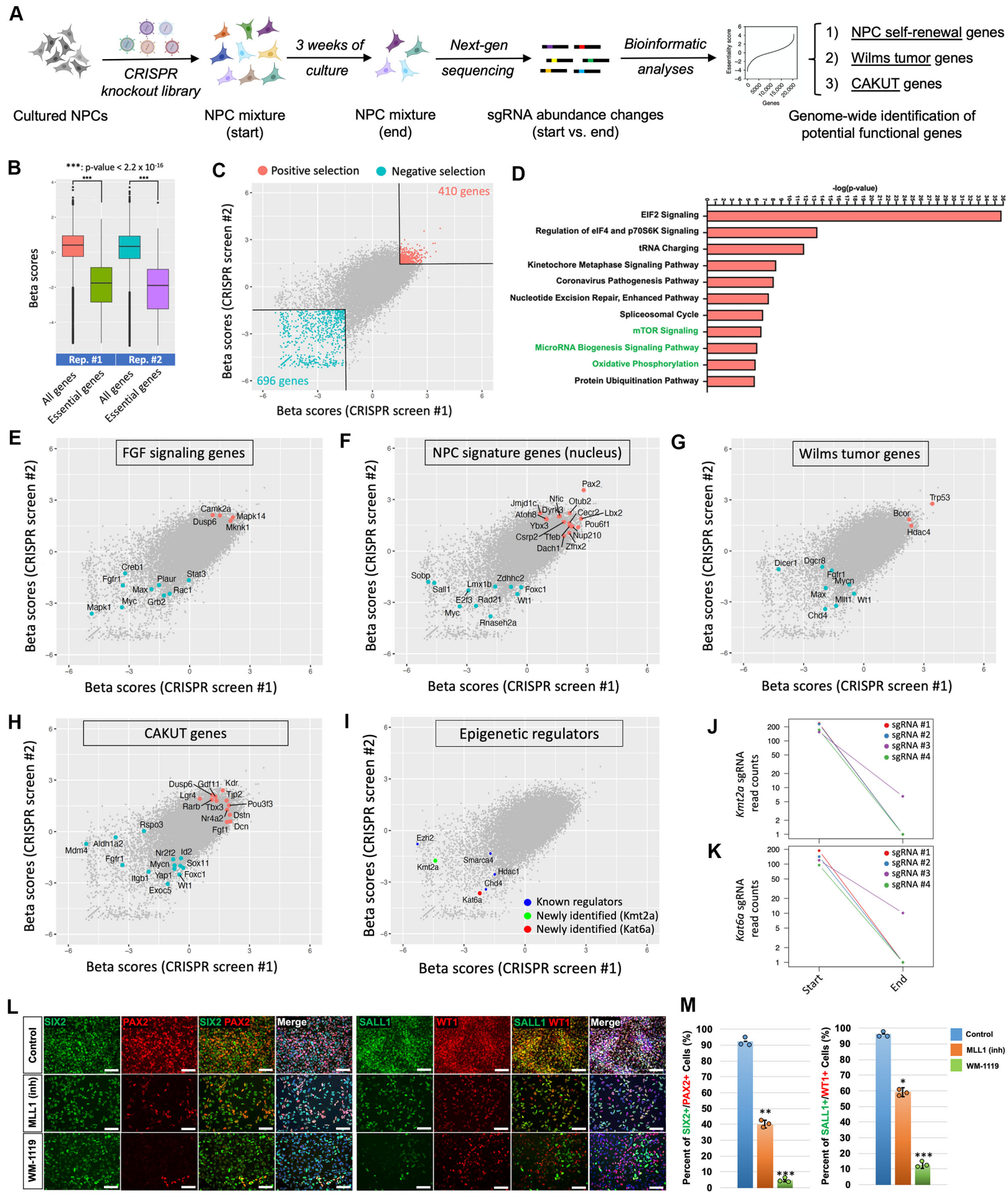


Figure 3. Genome-wide CRISPR screen in the NPC lines identify functional genes for kidney development and disease.

(A) Schematic diagram illustrates the workflow of genome-wide CRISPR knockout screen in mNPC lines.

(B) Box plot showing the distribution of beta scores of all genes or essential genes in two CRISPR screen replicates. Boxes, 25th to 75th percentiles; whiskers, 1st to 99th percentiles.

(C) MAGeCKFlute scatterplots of beta scores showing common positively and negatively selected genes from two CRISPR screen replicates.

(D) Top 11 enriched ingenuity pathway analysis (IPA) Canonical Pathways from CRISPR screen replicate #1.

(E–I) MAGeCKFlute scatterplots of beta scores from two CRISPR screen replicates showing FGF signaling related genes (E), NPC signature genes that encode nucleus-localizing proteins (F), Wilms tumor-related genes (G), CAKUT-related genes (H), and genes that regulate epigenetic mechanisms (I).

(J and K) Normalized read counts of 4 individual sgRNAs targeting *Kmt2a* (J) and *Kat6a* (K) at the start and the end of the CIRPSR screen.

(L and M) Immunofluorescence analyses (L) and quantification (M) of the expression of SIX2, PAX2, SALL1, and WT1 in mNPCs after treated with KMT2A inhibitor MLL1 (inh), or KAT6A inhibitor WM-1119, for 8 days. Scale bars, 50 μ m.

Data are presented as mean \pm SD. Each column represents counts from three biological replicates (n=3). The significance was determined by two-tailed unpaired Student's t tests; ns, not significant; *, p<0.05; **, p<0.01; ***, p<0.001.

See also Figure S4 and Tables S5-11.

Figure 4

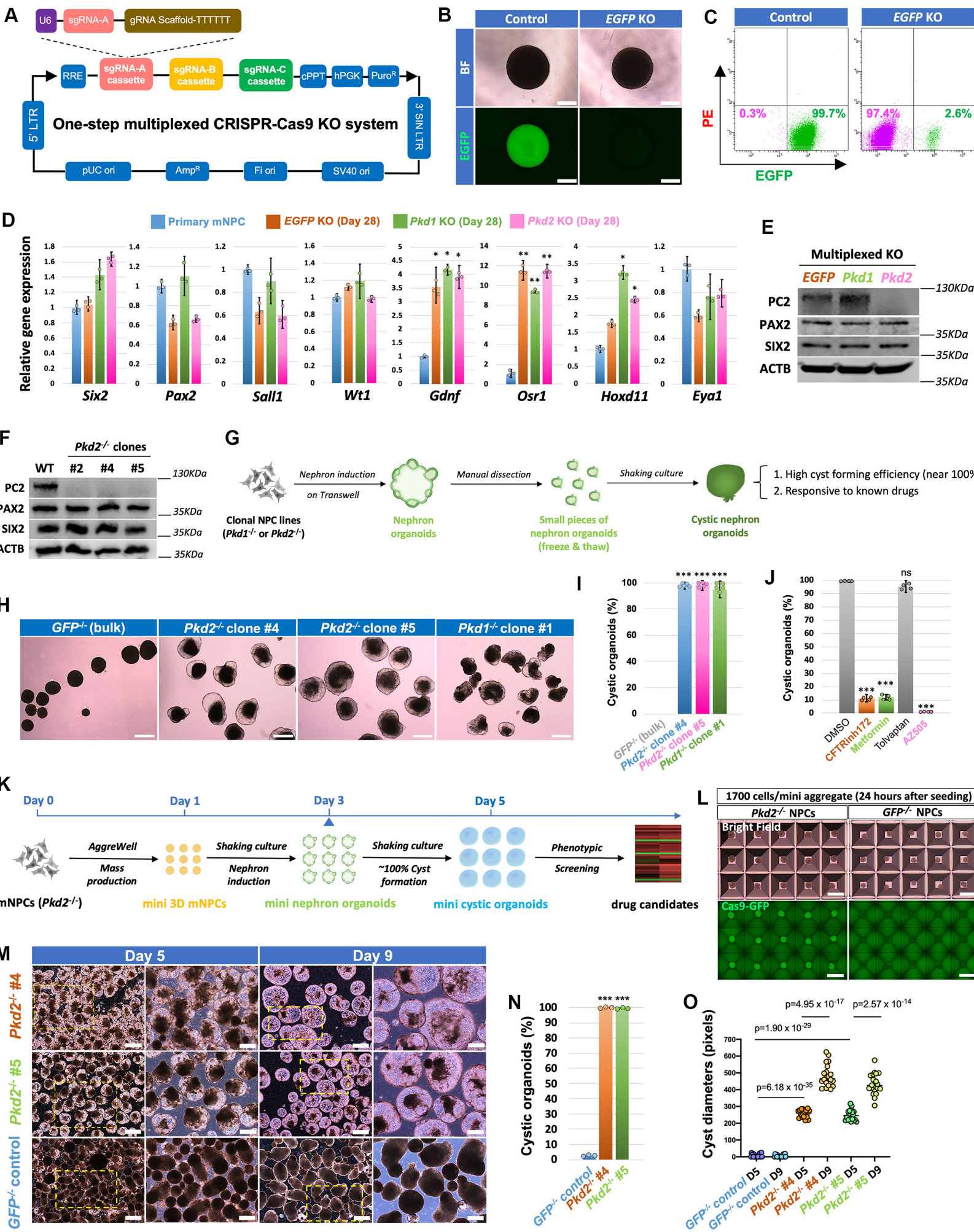


Figure 4. Rapid, efficient, and scalable PKD modeling from genome-edited mouse NPCs.

(A) Schematic showing the lentiviral vector design for one-step multiplexed CRISPR-Cas9 knockout (KO).

(B) Bright-field and EGFP images of aggregated Cas9-GFP mNPCs 7 days upon infection of lentivirus targeting *EGFP* gene and puromycin selection. Empty lentiviral vector without sgRNA was used as control. Scale bars, 200 μ m.

(C) Flow cytometry analysis of EGFP expression in control (left) or *EGFP* KO (right) Cas9-GFP mNPCs.

(D) qRT-PCR analysis for various NPC marker genes as indicated in bulk *EGFP*^{-/-}, *Pkd1*^{-/-}, and *Pkd2*^{-/-} NPC lines 28 days after lentiviral infection and puromycin selection. Primary NPC sample was used as control.

(E) Western blot analysis of bulk *EGFP*^{-/-}, *Pkd1*^{-/-}, and *Pkd2*^{-/-} mNPC lines (day 28 of culture after lentiviral infection) for PC2, PAX2, and SIX2, and beta-actin (ACTB) expression.

(F) Western blot analysis of *Pkd2*^{-/-} clonal mNPC lines for PC2, PAX2, and SIX2, and beta-actin (ACTB) expression. Wild-type (WT) mNPC line without genome-editing, cultured for a similar time period, was used as control.

(G) Schematic of the experimental protocol for deriving cystic nephron organoid model from *Pkd1*^{-/-} or *Pkd2*^{-/-} clonal mNPC lines.

(H) Bright-field images showing cyst formation in nephron organoids derived from *Pkd1*^{-/-} or *Pkd2*^{-/-} clonal mNPC lines. mNPC line with *EGFP* KO in bulk was used as control. Scale bars, 200 μ m.

(I) Quantification of the percentages of cystic organoids in samples shown in (H).

(J) Percentages of cystic organoids in *Pkd2*^{-/-} clonal mNPC line-derived nephron organoids treated with DMSO (control) or various drugs as indicated.

(K) Schematic of the experimental protocol for generating scalable mini cystic nephron organoids from *Pkd2*^{-/-} clonal mNPC lines for high-throughput drug screening.

(L) Bright-field and GFP images showing mini 3D mNPC aggregates upon seeding onto Aggrewell plates overnight, from *EGFP*^{-/-} or *PKD2*^{-/-} *Cas9-EGFP* genetic backgrounds. Scale bars, 500 μ m.

(M) Bright-field images showing cyst growth at 5 days and 9 days after shaking culture using protocol described in (K). Scale bars under each timepoint, 500 μ m (left panels) and 200 μ m (right panels).

(N and O) Quantification of cystic organoid percentages (N) and cyst diameters (O) for samples from (M).

Data are presented as mean \pm SD. Each column represents counts from three biological replicates (n=3). The significance was determined by two-tailed unpaired Student's t tests; ns, not significant; *, p<0.05; **, p<0.01; ***, p<0.001.

See also Figures S5 and S6.

Figure 5

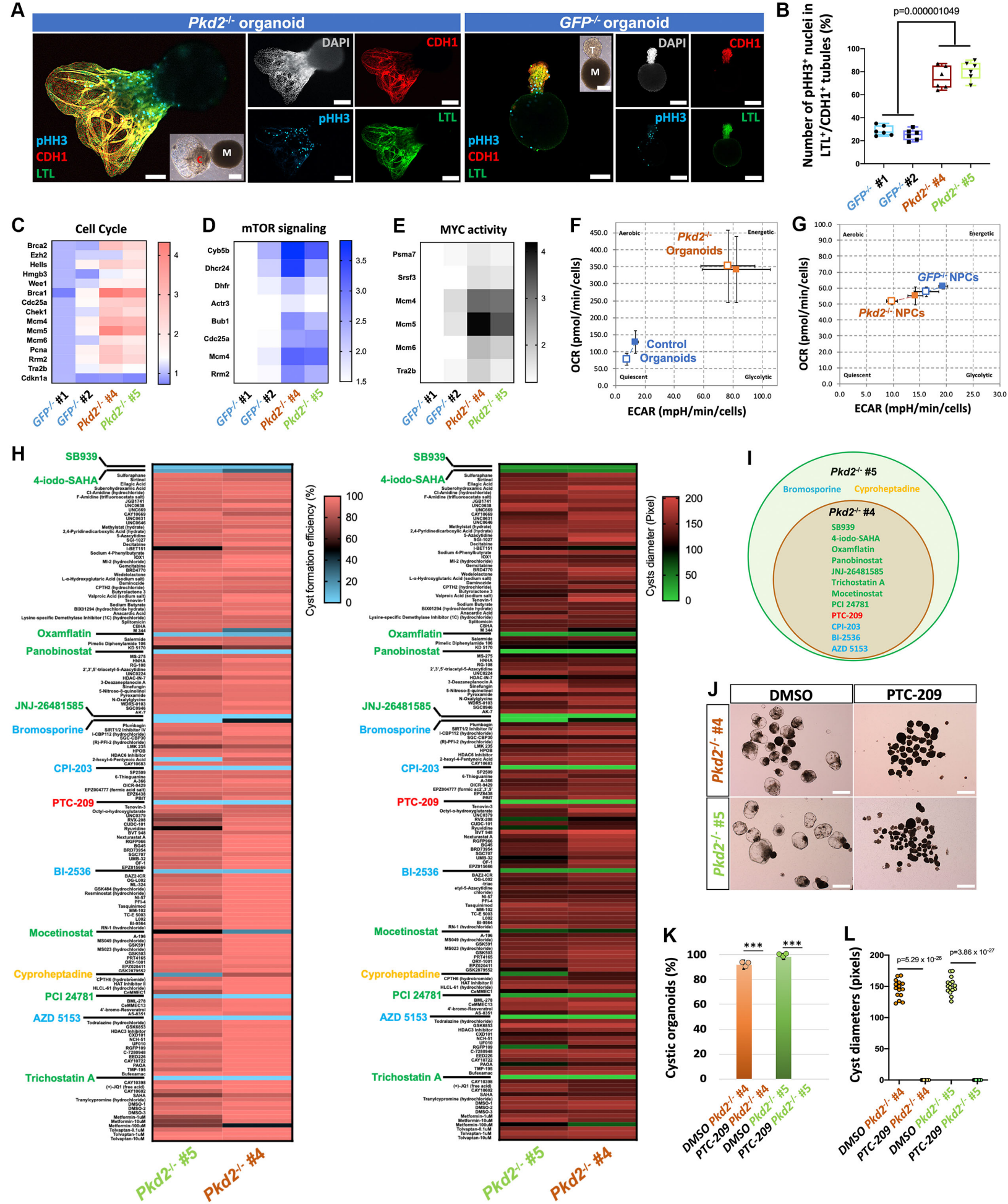


Figure 5. Drug screening identifies PTC-209 as a potential candidate for PKD treatment.

(A) Immunofluorescence analysis of *Pkd2*^{-/-} or *GFP*^{-/-} mini nephron organoids for pHH3, LTL and CDH1. C, cystic portion; M, mesenchymal portion; T, tubule portion. Scale bars, 100 μ m.

(B) Quantification of the numbers of pHH3⁺ nuclei in LTL⁺/CDH⁺ cells from *Pkd2*^{-/-} or *GFP*^{-/-} mini nephron organoids.

(C–E) Heat map presentation of cell cycle (C), mTOR signaling (D), and MYC activity (E) associated gene expression levels as determined by qRT-PCR, in *Pkd2*^{-/-} or *GFP*^{-/-} mini nephron organoids.

(F and G) Metabolic analyses of OCR and ECAR in *Pkd2*^{-/-} or *EGFP*^{-/-} mini nephron organoids (F) and *Pkd2*^{-/-} or *EGFP*^{-/-} NPCs (G) using Seahorse assays. Blank boxes indicate baseline levels and filled boxes indicate stressed levels upon oligo/FCCP treatment.

(H) Heat maps showing the quantification of drug screening results in terms of cyst formation efficiency (left) and cyst diameter (right) using mini PKD organoid models derived from two clonal *Pkd2*^{-/-} mNPC lines #4 and #5. Identified HDAC inhibitor hits are shown in green, and BRD4 inhibitors are shown in blue.

(I) Venn diagram showing the common drug candidates identified through drug screening from *Pkd2*^{-/-} #4 and #5 mNPC line-derived mini PKD organoids.

(J) Bright-field images showing mini PKD organoids derived from *Pkd2*^{-/-} #4 and #5 NPC lines, treated with DMSO (control) and PTC-209, during the drug screening. Scale bars, 500 μ m.

(K and L) Quantification of cyst organoid percentages (K) and cyst diameter (L) in samples shown in (J).

Data are presented as mean \pm SD. Each column represents counts from three biological replicates (n=3). The significance was determined by two-tailed unpaired Student's t tests; ns, not significant; *, p<0.05; **, p<0.01; ***, p<0.001.

See also Figures S7 and S8.

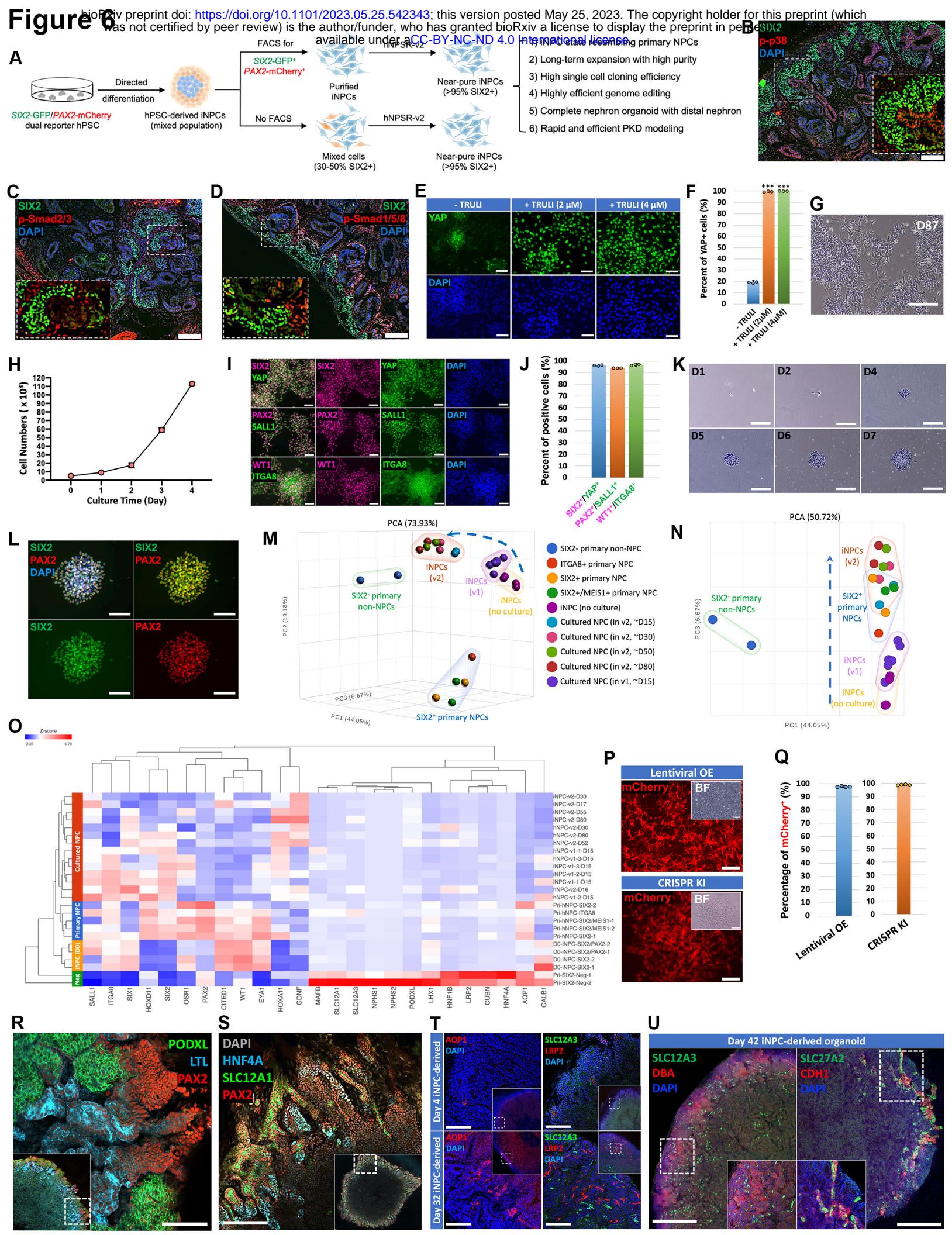


Figure 6. YAP activation captures human NPCs with restored distal nephron differentiation potential.

(A) Schematic showing the derivation of long-term expandable iNPC lines from hPSCs and its versatile applications.

(B–D) Immunofluorescence analyses of 11.3-week human fetal kidney sections for SXI2, p-p38 (B), p-SMAD2/3 (C), and p-SMAD1/5/8 (D). Scale bars, 50 μ m.

(E and F) Immunofluorescence analyses (E) and quantification (F) of YAP expression in iNPCs cultured in hNPSR-v1 medium supplemented with 0, 2, or 4 μ M TRULI for 6 days. Scale bars, 50 μ m.

(G) Bright-field image of iNPCs cultured in hNPSR-v2 medium for 87 days. Scale bar, 100 μ m.

(H) Growth curve of iNPCs cultured in hNPSR-v2 in a typical 4-day passage cycle starting from 5,000 cells.

(I and J) Immunofluorescence analyses (I) and quantification (J) of iNPCs cultured in hNPSR-v2 medium for 21 days for various NPC marker genes as indicated. Scale bars, 100 μ m.

(K) Time-course bright-field images showing clonal expansion of iNPCs from one single cell in hNPSR-v2 medium. Scale bars, 100 μ m.

(L) Immunofluorescence analysis of a single cell iNPC clone for SIX2 and PAX2. Scale bars, 50 μ m.

(M and N) 3D (M) and 2D (N) PCA plots of bulk RNA-seq data.

(O) Heatmap showing gene expression of selected marker genes for undifferentiated NPCs and differentiated kidney cell types, in primary and cultured NPCs, as well as FACS-purified SIX2⁺ or SIX2⁺/PAX2⁺ iNPCs without further culture (D0-iNPC-SIX2 and D0-iNPC-SIX2/PAX2). Primary SIX2-negative non-NPCs (Pri-SIX2-Neg) isolated from human fetal kidneys were used as negative controls.

(P and Q) Bright field (BF) and fluorescence images (P) and quantification (Q) of mCherry expression in iNPCs upon lentiviral overexpression of mCherry (lentiviral OE), or targeted

CRISPR/Cas9 knock-in of mCherry-expressing cassette into *AAVS1* allele (CRISPR KI). Scale bars, 50 μ m.

(R and S) Whole-mount immunofluorescence analyses of human nephron organoids generated from iNPCs cultured in hNPSR-v2 medium for 42 days for various nephron marker genes as indicated. Scale bars, 200 μ m.

(T) Whole-mount immunofluorescence analyses of human nephron organoids generated from iNPCs cultured in hNPSR-v2 for 4 days (upper panels) or 32 days (lower panels) for various nephron marker genes as indicated. Scale bars, 200 μ m.

(U) Whole-mount immunofluorescence analyses of human nephron organoid generated from iNPCs cultured in hNPSR-v2 medium for 42 days for various nephron marker genes as indicated. Scale bar, 200 μ m.

Data are presented as mean \pm SD. Each column represents counts from three biological replicates (n=3). The significance was determined by two-tailed unpaired Student's t tests; ns, not significant; *, p<0.05; **, p<0.01; ***, p<0.001.

See also Figures S9, S10, and Tables S12 and 13.

Figure 7

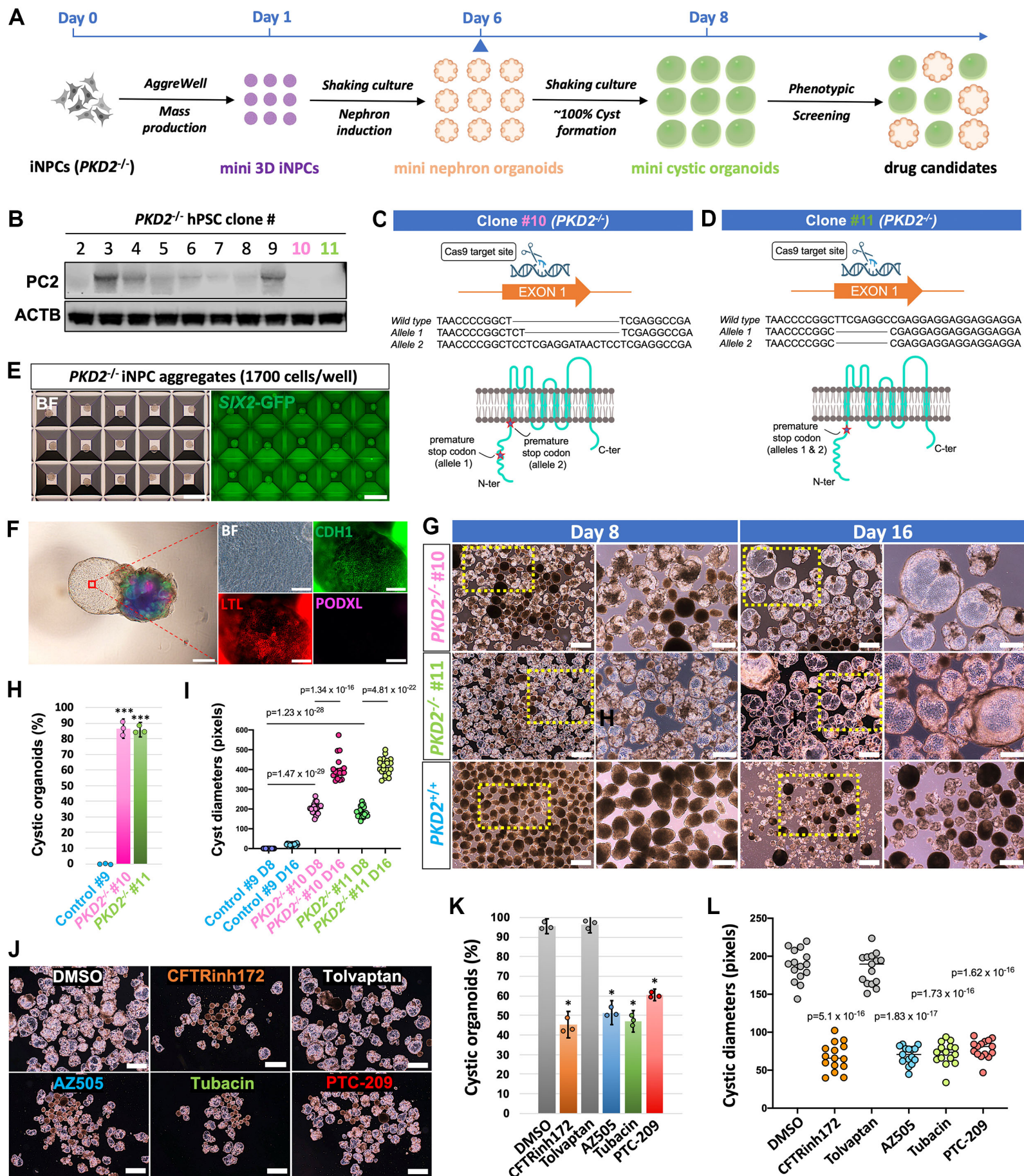


Figure 7. Rapid, efficient, and scalable PKD modeling from genome-edited human NPCs.

(A) Schematic showing the experimental procedures for generating PKD organoids directly from expandable *PKD2*^{-/-} iNPCs.

(B) Western blot analysis of PC2 expression in different candidate *PKD2*^{-/-} single cell hPSC clones.

(C and D) Schematic showing CRISPR/Cas9-mediated random insertions or deletions (indels) on the first exon of *PKD2* gene, leading to double allele premature termination of *PKD2* transcription in *PKD2*^{-/-} clonal iNPC lines #10 and #11.

(E) Bright-field and GFP images of mini *PKD2*^{-/-} *SIX2*-GFP iNPC aggregates upon seeding onto Aggrewell plate overnight. Scale bars, 500 μ m.

(F) Bright-field (BF) and immunofluorescence images of a cystic nephron organoid derived from *PKD2*^{-/-} iNPCs. Right panels show enlarged images of the boxed cystic area from the left panel. Scale bars, 500 μ m (left panel) and 100 μ m (right panels).

(G) Bright-field images showing rapid cyst formation and continuous growth in the mini PKD organoids, derived from *PKD2*^{-/-} iNPC lines #10 and #11. Right panels under each time point show enlarged pictures of the boxed areas from the left panels. Scale bars, 500 μ m and 200 μ m (enlarged pictures).

(H and I) Quantification of cystic organoid percentages and cyst diameters for samples shown in (G).

(J) Bright-field images of *PKD2*^{-/-} iNPC-derived mini cystic PKD organoids treated with various known drugs for PKD, and PTC-209. Scale bars, 500 μ m.

(K and L) Quantification of cystic organoid percentages and cyst diameters for samples shown in (J).

Data are presented as mean \pm SD. Each column represents counts from three biological replicates (n=3). The significance was determined by two-tailed unpaired Student's t tests; ns, not significant; *, p<0.05; **, p<0.01; ***, p<0.001.

STAR METHODS

KEY RESOURCES TABLE

REAGENT or RESOURCE	SOURCE	IDENTIFIER
Antibodies		
Rabbit Monoclonal anti-SIX1	Cell Signaling Technology	Cat# 12891, RRID: AB_2753209
Rabbit Polyclonal anti-SIX2	Proteintech	Cat# 11562-1-AP, RRID: AB_2189084
Mouse Monoclonal anti-SIX2	Abnova	Cat# H00010736-M01, RRID: AB_436993
Mouse Monoclonal anti-SALL1	R&D Systems	Cat# PP-K9814-00, RRID: AB_2183228
Rabbit Monoclonal anti-WT1	Abcam	Cat# ab89901, RRID: AB_2043201
Rabbit Polyclonal anti-PAX2	BioLegend	Cat# 901001, RRID: AB_2565001
Rabbit Polyclonal anti-PAX8	Proteintech	Cat# 10336-1-AP, RRID: AB_2236705
Mouse Monoclonal anti-MEIS1/2/3	Active Motif	Cat# 39795, RRID: AB_2750570
Rat Monoclonal anti-PODXL (mouse)	R&D Systems	Cat# MAB1556, RRID: AB_2166010
Mouse Monoclonal anti-PODXL (human)	R&D Systems	Cat# MAB1658, RRID: AB_2165984
Biotinylated Lotus Tetragonolobus Lectin (LTL)	Vector laboratories	Cat# B-1325, RRID: AB_2336558
Mouse Monoclonal anti-LRP2	MyBioSource	Cat# MBS690201
Biotinylated Dolichos Biflorus Agglutinin (DBA)	Vector laboratories	Cat# B-1035, RRID: AB_2314288
Rabbit Monoclonal anti-CDH1	Cell Signaling Technology	Cat# 3195, RRID: AB_2291471
Mouse Monoclonal anti-CDH1	BD Biosciences	Cat# 610182, RRID: AB_397581
Mouse Monoclonal anti-AQP1 (mouse)	Santa Cruz Biotechnology	Cat# sc-25287, RRID: AB_626694
Rabbit Monoclonal anti-AQP1 (human)	Abcam	Cat# ab168387, RRID: AB_2810992
Mouse Monoclonal anti-HNF4	R&D Systems	Cat# MAB4605
Goat Polyclonal anti-SLC12A1	Abcam	Cat# ab240542, RRID: AB_2910116
Rabbit Polyclonal anti-SLC12A3	Sigma-Aldrich	Cat# HPA028748-100UL, RRID: AB_10603886
Mouse Monoclonal anti-SLC27A2	Novus Biologicals	Cat# NBP2-37738
Rabbit polyclonal anti- SLC34A1 antibody	Novus Biologicals	Cat# NBP2-13328
Goat Polyclonal anti-ITGA8	R&D Systems	Cat# AF4076, RRID: AB_2296280

Rabbit Monoclonal anti-p-p38	Cell Signaling Technology	Cat# 4511, RRID: AB_2139682
Rabbit Monoclonal anti-p-SMAD2	Cell Signaling Technology	Cat# 18338, RRID: AB_2798798
Rabbit Monoclonal anti-p-Smad1/5/9	Cell Signaling Technology	Cat# 13820, RRID: AB_2493181
Rat Monoclonal anti-KRT8	DSHB	Cat# TROMA-I, RRID: AB_531826
Chicken Polyclonal anti-MAP2	Abcam	Cat# ab5392, RRID: AB_2138153
Rabbit polyclonal anti-NeuN	GeneTex	Cat# GTX16208
Mouse Monoclonal anti-Phospho-Histone H3 (Ser10) pH3	Cell Signaling Technology	Cat# 9706, RRID: AB_331748
Mouse Monoclonal anti-YAP	Santa Cruz Biotechnology	Cat# sc-101199, RRID: AB_1131430
Rabbit polyclonal anti-PC2	Baltimore PKD Core	Cat# Rabbit mAB 3374 CT-14/4
Mouse Monoclonal anti-β-Actin	Cell Signaling Technology	Cat# 3700, RRID: AB_2242334
Rabbit polyclonal anti-β-Tubulin	Cell Signaling Technology	Cat# 2146, RRID: AB_2210545
DAPI	Thermo Fisher Scientific	D1306, RRID: AB_2629482

Chemicals, peptides, and recombinant proteins

Activin A	Stemgent	Cat# 03-0001
SB431542	Reagents Direct	Cat# 21-A94
A83-01	Stemgent	Cat# 04-0014
BMP4	Stemgent	Cat# 03-0007
BMP7	R&D Systems	Cat# 354-BP-010
LDN-193189	Reagents Direct	Cat# 36-F52
CHIR99021	Reagents Direct	Cat# 27-H76
IWR-1	Sigma-Aldrich	Cat# 10161-5MG
Y-27632	Selleck Chemicals	Cat# S1049
PD0325901	Reagents Direct	Cat# 39-C68
FGF1	Peprotech	Cat# AF-100-17A
FGF2	Peprotech	Cat# AF-450-33
FGF7	Peprotech	Cat# 450-60
FGF8	Peprotech	Cat# AF-100-25
FGF9	Peprotech	Cat# 100-23
FGF10	Peprotech	Cat# AF-100-26
FGF20	Peprotech	Cat# 100-41
TNF-alpha	R&D Systems	Cat# 210-TA-020
VEGF	R&D Systems	Cat# 293-VE-010
HGF	Peprotech	Cat# 315-23
EGF	R&D Systems	Cat# 236-EG-200
JAK Inhibitor I	STEMCELL Technologies	Cat# 74022
Sphingosine-1-phosphate (S1P)	Sigma-Aldrich	Cat# S9666-1MG
Lysophosphatidic acid (LPA)	Sigma-Aldrich	Cat# L7260-1MG
SCF	R&D Systems	Cat# 255-SC-010
IGF-1	Sigma-Aldrich	Cat# I1271-.1MG

IGF-2	Peprotech	Cat# AF-100-12
Mouse LIF	Millipore	Cat# ESG1107
Human LIF	Millipore	Cat# LIF1050
All trans-Retinoic Acid	Santa Cruz Biotechnology	Cat# sc-200898
TTNPB	TOCRIS	Cat# 0761
SP600125	TOCRIS	Cat# 1496
SB202190	Axon Medchem	Cat# 1364
DAPT	Sigma-Aldrich	Cat# D5942-5MG
XMU-MP-1	Selleck Chemicals	Cat# S8334
Verteporfin	Selleck Chemicals	Cat# S1786
Forskolin	Sigma-Aldrich	Cat# F3917-10MG
GDNF	PeproTech	Cat# 450-10-50ug
PDGF-BB	R&D Systems	Cat# 220-BB-010
R-Spondin 1	R&D Systems	Cat# 4645-RS-100
AICAR	Sigma-Aldrich	Cat# A9978
TRULI	Gnedeva lab, USC	10mM-Stock
MOZ-IN-3	Cayman Chemical	Cat# 27402-1mg
WM-1119	Cayman Chemical	Cat# 30509-5mg
WDR5 degrader	Yali Dou lab, USC	10mM-Stock
MLL1 inhibitor	Yali Dou lab, USC	20mM-Stock
Epigenetics Screening Library (96-Well) (148 Compounds)	Cayman Chemical	Cat# 11076
Tolvaptan	Selleck Chemicals	Cat# S2593
Metformin	TOCRIS	Cat# 2864
CFTRinh172	Cayman Chemical	Cat# 15545-5mg
AZ-505	Cayman Chemical	Cat# 16875-1mg
Tubacin	Cayman Chemical	Cat# 13691-1mg
PTC-209	Cayman Chemical	Cat# 16277-5mg

Critical commercial assays

TRIzol Reagent	Thermo	Cat# 15596026
Direct-zol RNA MicroPrep Kit	Zymo Research	Cat# R2062
DNA/RNA Shield	Zymo Research	Cat# R1100-50
Quick-RNA Microprep Kit	Zymo Research	Cat# R1051
iScript Reverse Transcription Supermix	Bio-Rad	Cat# 1708841
Ssoadvanced™ Universal SYBR	Bio-Rad	Cat# 1725274
AzuraView GreenFast qPCR Blue Mix LR	Azura Genomics	Cat# AZ-2320
TSA Plus Cyanine 3 Evaluation Kit	PerkinElmer	Cat# NEL744E001KT
KAPA Stranded mRNA-Seq Kit	KAPA Biosystems	Cat# KK8420
CyQUANT® Cell Proliferation Assay Kit	Invitrogen	Cat# C7026
AggreWell™800 6-well Starter Kit	STEMCELL Technologies	Cat# 34860
AggreWell™800 24-well Plate Starter Kit	STEMCELL Technologies	Cat# 34850

Deposited data

Bulk RNA-seq of mouse and human NPC	NCBI's GEO	GSE230707 (reviewer token: wnoxmwcuflkbpiz)
Bulk RNA-seq of primary mouse NPC ¹	NCBI's GEO	GSE78772
Bulk RNA-seq of primary human NPC ²	NCBI's GEO	GSE102230
Bulk RNA-seq of primary human NPC ³	NCBI's GEO	GSE73867

Experimental models: Human tissues		
Human fetal kidney tissues (9-13 weeks)	USC and CHLA	N/A
Experimental models: hPSC lines		
<i>SIX2-GFP</i> H1 hESC	This study	N/A
<i>SIX2-GFP/PAX2-mCherry</i> H1 hESC	This study	N/A
<i>SIX2-GFP PKD2^{-/-}</i> H1 hESC	This study	N/A
Experimental models: Organisms/strains		
Swiss Webster mice	Taconic Biosciences	Model # SW-F
<i>Six2^{tm3(EGFP/cre/ERT2)Amc}</i> mice (<i>Six2^{GCE}</i>)	The Jackson Laboratory	JAX # 009600 RRID: IMSR_JAX:009600
<i>Wnt4^{tm2(EGFP/cre/ERT2)Amc}</i> mice (<i>Wnt4^{GCE}</i>)	The Jackson Laboratory	JAX # 032489 RRID: IMSR_JAX:032489
<i>B6;129S4-Foxd1^{tm1(GFP/cre)Amc}</i> /J mice (<i>Foxd1^{GC}</i>)	The Jackson Laboratory	JAX # 012463 RRID: IMSR_JAX:012463
<i>Gt(ROSA)26Sor^{tm1.1(CAG-cas9*,-EGFP)Feh}</i> mice	The Jackson Laboratory	JAX # 026179 RRID: IMSR_JAX:026179
<i>Tg(Hoxb7-Venus*)17Cos</i> mice	The Jackson Laboratory	JAX # 016252 RRID: IMSR_JAX:016252
<i>Gt(ROSA)26Sor^{tm14(CAG-tdTomato)Hze}</i> mice	The Jackson Laboratory	JAX # 007908 RRID: IMSR_JAX:007908
Oligonucleotides		
gRNA-EGFP_1: 5'-AAGGGCGAGGAGCTGTTCAC-3'	Zuo et al., 2017	N/A
gRNA-EGFP_2: 5'-CTGAAGTTCATCTGCACCAAC-3'	Zuo et al., 2017	N/A
gRNA-EGFP_3: 5'-GGAGCGCACCATCTTCTTCA-3'	Zuo et al., 2017	N/A
gRNA-Pkd1_1: 5'-GCTGCGCTGACGATGCCGCT-3'	This study	N/A
gRNA-Pkd1_2: 5'-CTGGCCGGAGACCCTGGGCG-3'	This study	N/A
gRNA-Pkd1_3: 5'-AGCGGCCGGAGCAATTGACG-3'	This study	N/A
Primer_F_Pkd1_Sanger_seq_genotype (CCCTCCTGAAC TGCGGGCT)	This study	N/A
Primer_R_Pkd1_Sanger_seq_genotype (GGACCCAGTCATGATGCTCA)	This study	N/A
gRNA-Pkd2_1: 5'-CGAGATGGAGCGCATCCGGC-3'	This study	N/A
gRNA-Pkd2_2: 5'-TCGCCCCGCGCCGAGCGTC-3'	This study	N/A
gRNA-Pkd2_3: 5'-AGTGGCGCCGGCAGTCGG-3'	This study	N/A
Primer_F_Pkd2_Sanger_seq_genotype	This study	N/A

(GCAAGCTACCCCGTAGGAATG)		
Primer_R_Pkd2_Sanger_seq_genotype	This study	N/A
(GCGCAGGCAGTTGTCAAGC)		
gRNA-PKD2: 5'- CCGCGATAACCCCGGCTTCG-3'	This study	N/A
Primer_F_PKD2_Sanger_seq_genotype	This study	N/A
(GGAAGAAAGGAACATGGCTCC)		
Primer_R_PKD2_Sanger_seq_genotype	This study	N/A
(TCTACGTCCATCTCCACAC)		
gRNA-SIX2: 5'- GGGCTCTAGAACCCATTG-3'	This study	N/A
gRNA-PAX2: 5'- ATGACCGCCACTAGTTACCG-3'	This study	N/A
<hr/>		
Recombinant DNA		
lentiCRISPR v2		Addgene: #52961 RRID:
lentiGuide-Puro		Addgene_52961 Addgene # 52963 RRID:
plKO.1-TRC		Addgene_52963 Addgene # 10878 RRID:
lentiCas9-Blast		Addgene_10878 Addgene, # 52962 RRID:
The Brie genome-wide CRISPR knockout library		Addgene_52962 Addgene # 73632 RRID:
EF1a_mCherry_P2A_Hygro		Addgene_73632 Addgene, # 135003 RRID:
pAAVS1-P-CAG-mCherry		Addgene_135003 Addgene, # 80492 RRID:
pxAT2		Addgene_80492 Addgene, # 80494 RRID:
pcAS9_GFP		Addgene_80494 Addgene # 44719 RRID:
Nanog-2A-mCherry		Addgene_44719 Addgene # 59995 RRID:
pSpCas9(BB)-2A-Puro (PX459) V2.0		Addgene_59995 Addgene # 62988 RRID:
plKO-Puro-gRNA-EGFPx3	This paper	Addgene_62988 N/A
plKO-Puro-gRNA-Pkd1x3	This paper	N/A
plKO-Puro-gRNA-Pkd2x3	This paper	N/A
<hr/>		
Software and algorithms		

ImageJ (version: 2.1.0)	Schneider et al.	https://imagej.nih.gov/ij/ ; RRID: SCR_003070
GraphPad Prism software (version: 9.1.0)	GraphPad Prism	GraphPad Prism (https://graphpad.com) ; RRID: SCR_015807
FlowJo software (version: 10.0.0)	FlowJo	FlowJo (https://www.flowjo.com/) ; RRID: SCR_008520
Partek Flow Genomic Analysis software	Partek Genomics Suite	Partek Genomics Suite (http://www.partek.com) RRID: SCR_011860
RStudio software	RStudio	RStudio (https://posit.co/) RRID: SCR_000432
Ingenuity Pathway Analysis software	QIAGEN	Ingenuity Pathway Analysis (http://www.ingenuity.com/products/pathway_analysis.html) RRID: SCR_008653
SnapGene software	SnapGene	SnapGene (http://www.snapgene.com) RRID: SCR_015052
ZEN Digital Imaging for Light Microscopy	ZEISS	ZEN Digital Imaging for Light Microscopy (http://www.zeiss.com/microscopy/en_us/products/microscope-software/zen.html#introduction) RRID: SCR_013672
Olympus Cellsens Standard software	Olympus	Olympus cellSens Software (http://www.olympus-lifescience.com/en/software/cellsens) RRID: SCR_014551
Wave software	Agilent Technologies	Seahorse Wave (http://www.agilent.com/en-us/products/cell-analysis-(seahorse)/software-download-for-wave-desktop)

) RRID: SCR_014526

RESOUCE AVAILABILITY

Lead contact

Further information and requests for resources and reagents should be directed to and will be fulfilled by the lead contact, Zhongwei Li (zhongwei.li@med.usc.edu).

Materials availability

Cell lines, plasmids, and other unique resources generated in this study are available from the lead contact, Zhongwei Li (zhongwei.li@med.usc.edu), with a completed Materials Transfer Agreement.

Data and code availability

RNA-seq data have been deposited at GEO (GSE230707) with reviewer security token: wnoxmwcufjkbpiz. The data will be made publicly available upon publication. Any additional information required to reanalyze the data reported in this paper is available from the lead contact upon request.

EXPERIMENTAL MODEL AND SUBJECT DETAILS

Human tissues

All human fetal kidney samples were collected under Institutional Review Board approval at both the University of Southern California and Children's Hospital Los Angeles (USC-HS-13-0399 and

CHLA-14-2211). Consent for tissue donation was obtained after the patient had already made the decision for pregnancy termination by Dilation and Curettage or Dilation and Evacuation and was obtained by a different clinical staff member than the physician performing the procedure. All tissues were de-identified, and the only clinical information collected was gestational age and the presence of any maternal or fetal diagnoses.

Resource	Source	Identifier
Human fetal kidney tissues (9-13 weeks)	USC and CHLA	N/A

Mice

All animal work was performed under Institutional Animal Care and Use Committee approval (USC IACUC Protocol # 20829). Swiss Webster mice were purchased from Taconic Biosciences (Model # SW-F). *Six2*^{tm3(EGFP/cre/ERT2)Amc} mice (*Six2*^{GCE}, JAX # 009600), *Wnt4*^{tm2(EGFP/cre/ERT2)Amc} mice (*Wnt4*^{GCE}, JAX # 032489), *Foxd1*^{tm1(GFP/cre)Amc} mice (*Foxd1*^{GC}, JAX# 012463), *Gt(ROSA)26Sor*^{tm1.1(CAG-cas9*,-EGFP)Fehz} mice (JAX # 026179), and *Tg(Hoxb7-Venus*)17Cos* mice (JAX # 016252) were kindly shared from Dr. Andrew McMahon. *Gt(ROSA)26Sor*^{tm14(CAG-tdTomato)Hze} mice (tdTomato reporter mice, JAX # 007908) were kindly shared from Dr. Kenneth Hallows. *Six2-tdTomato* (*Six2-tdT*) mice were generated through crossing *Six2*^{GCE} mice and tdTomato reporter mice. *Wnt4-tdTomato* (*Wnt4-tdT*) mice were generated through crossing *Wnt4*^{GCE} mice and tdTomato reporter mice.

hPSC lines

Experiments using hPSCs were approved by the Stem Cell Oversight Committee (SCRO) of University of Southern California under protocol # 2018-2. Human pluripotent stem cells are routinely cultured in mTeSR1 (STEMCELL Technologies #85850) or mTeSR1 Plus (STEMCELL Technologies #100-0276) medium in monolayer culture format coated with Matrigel and passaged

using dispase as previously described ¹, or using Versene Solution (Thermo Fisher # 15040066) following manufacturer's protocols.

Resource	Source	Identifier
<i>SIX2-GFP</i> H1 hESC	This study	N/A
<i>SIX2-GFP/PAX2-mCherry</i> H1 hESC	This study	N/A
<i>SIX2-GFP PKD2^{-/-}</i> H1 hESC	This study	N/A

METHOD DETAILS

Deriving clonal expandable NPC lines from any mouse strain with mNPSR-v2 medium

Deriving NPC lines from *Six2-GFP* mice

Timed pregnant E12.5-E18.5 kidneys were isolated from *Six2-GFP* (*Six2*^{GCE}, JAX # 009600) mouse embryos, and then the kidneys were minced into small pieces. The minced kidney pieces were transferred into 1.5mL Eppendorf tubes and spun down at 300 g for 3 minutes. (Note that we aliquoted the kidney pieces into multiple tubes to ensure the volume of the tissue pellet after centrifugation was less than 100 μ l per tube to ensure best dissociation). The dissection medium was then carefully aspirated. The kidney pieces were then washed once with sterile PBS. 500 μ L of pre-warmed Accumax Cell Dissociation Solution (Innovative Cell Technologies, Cat. No. AM-105) was added to the tube to resuspend the kidney pieces. The tube was incubated in 37°C incubator for 20~22 minutes. 500 μ L 10% FBS medium (10% FBS in DMEM) was added to the tube, and then GENTLY pipetted up and down 20 to 25 times to further dissociate the kidney pieces. The tube was spun down and the supernatant was then removed. FACS medium (cold PBS with 2% FBS) was added to resuspend the cell pellet and the cell suspension was filtered

through 40 μ m cell strainer (Greiner bio-one, Cat. No. 542040) to remove cell clumps before FACS to sort out *Six2*-GFP $^+$ NPCs. Purified *Six2*-GFP $^+$ NPCs were counted with TC20TM Automated Cell Counter (Bio-Rad, Cat. No. 1450102), and then cultured in mNPSR-v2 medium (Table S2) to establish NPC lines. Take 96-well plate for example, we counted and seeded 5,000 FACS-purified NPCs into one Matrigel-coated well with 100 μ l mNPSR-v2 medium. The medium was refreshed 2 days after cell seeding. When NPCs grew to 80-90% confluent (on day 3 or day 4), the culture medium was removed, and the cells were washed once with 100 μ l PBS, and then dissociated with 50 μ l pre-warmed Accumax. The cells were incubated with Accumax for 8 mins, and then 150 μ l 10% FBS medium was added to neutralize Accumax. The medium was pipetted up and down GENTLY for 5-7 times to make single cell suspension, which was then seeded at 1:20-1:30 passage ratio to a new well in 96-well plate. Change medium 2 days after seeding. On day 3 or day 4, the cells grew to 80-90% confluent and can be passaged again using the same protocol described above. (Note, for coating with Matrigel (R&D Systems, # 3433-010-01) in one well of 96-well plate, dissolve 1 mg Matrigel into 25 ml cold DMEM/F12, and then aliquot 100 μ l medium into each well. The plate is then incubated in 37°C for at least 1-2 hours before the coating medium is aspirated followed by cell seeding.)

Deriving NPC lines from E11.5 metanephric mesenchyme (MM)

E11.5 kidneys were isolated and MM was manually dissected out from the E11.5 kidneys following our previously described protocol to isolate E11.5 UB and MM (Zeng et al., 2021). 20 isolated MM were pooled together and dissociated in 500 μ l Accumax for 8-10 minutes (scale it down if less MM were isolated) before 500 μ l 10% FBS medium was added to neutralize Accumax. The medium was then pipetted up and down GENTLY for 7-10 times to dissociate the MM into single cells. 5,000 cells were then seeded into one well in a Matrigel-coated 96-well plate (scale

up or down based on the surface area, if different culture format was used) in mNPSR-v2 medium to derive NPC line, using similar protocols described above starting from *Six2*-GFP⁺ NPCs.

Deriving NPC lines from whole kidneys

E12.5-E15.5 kidneys were isolated, minced into small pieces, and dissociated in Accumax as described above for dissociating E12.5-E18.5 *Six2*-GFP kidneys. 5,000 cells were then seeded into one well in a Matrigel-coated 96-well plate (scale up or down if different culture format was used) in mNPSR-v2 medium to derive NPC line, using similar protocols described above starting from *Six2*-GFP⁺ NPCs. Note that, different from NPC line derivation from *Six2*-GFP⁺ NPCs, or from isolated E11.5 MM, whole kidney cells need to go through 2-3 passages to enrich the NPC population in the culture before a stable NPC line can be established with 90-95% purity.

Deriving single cell clonal mouse NPC lines

NPC lines can be derived from FACS-purified *Six2*-GFP⁺ NPCs, isolated E11.5 MM, or whole kidney cells as described above. When NPC lines are stably established, single cell clonal NPC lines can be generated. For that, when the NPC lines grew to around 80% confluence, the cells were dissociated into single cells following the protocol described above for passaging NPCs. The cells were counted and seeded into Matrigel-coated 96-wells at the density 0.5 cell per well with 100 µl mNPSR-v2 medium so that most wells would have either one single cell or no cell (day 0). On day 3, 50 µl used medium was removed, and 100 µl fresh medium was added. On day 6, the used medium was completely removed and 100 µl fresh medium was added. On day 9, NPC clones were clearly observed under the microscope in about 30% of the wells seeded. Cells in these wells were dissociated following our protocol described above, and all the cells were seeded into another 96-well. On day 11, the cells reached around 80-90% confluence and were passaged routinely thereafter every 3 days as described above. To determine cloning efficiency, 60 wells of a 96-well plate were seeded with single cell NPC following the method mentioned above (D0). On

day 3, the wells containing clusters of cells from a single cell were labeled and counted, and the wells without any cell were discontinued. On day 9, the number of wells grown at least 50% confluence was counted. Cloning efficiency was calculated by using the number of wells recorded on day 9 divided by the number of wells recorded on day 3, from three independent experiments.

Generation of mouse nephron organoids from mouse NPC lines

mNPCs cultured in mNPSR-v2 medium were dissociated into single cells using Accutase as described above. 30,000 cells were seeded into one well of a U-bottom 96-well plate (Thermo Fisher Scientific, # 174929) and cultured with 100 µl mNPSR-v2 medium overnight for cells to aggregate. Nephron organoids were formed thereafter following the protocol we described previously¹. Briefly, on the next day (Day 0), 3D NPC aggregates were transferred onto 6-well format transwell membrane (Corning, # 3450) with 1.2 mL KR5-CF medium at the bottom chamber and cultured for 2 days. On Day 2, change medium to 1.2 mL KR5 medium and change medium every other day. Samples were harvested on Day 7 for various assays.

KR5 medium

Basal medium: DMEM/F12 (1:1) (1X), Invitrogen, Cat. No. 11330-032.

Supplements:

Reagent Name	Company	Cat. No.	Final Concentration
GlutaMAX-I (100X)	Invitrogen	35050-079	1X
MEM NEAA (100X)	Invitrogen	11140-050	1X
2-Mercaptoethanol (55mM)	Invitrogen	21985-023	0.1 µM
Pen Strep (100X)	Invitrogen	15140-122	1X
KSR (KnockOut™ Serum Replacement)	Invitrogen	10828-028	5 %

KR5-CF medium

KR5 medium with 4.5 μ M CHIR99021 (C) and 200 ng/mL FGF2 (F).

Spinal cord induction assay

After mNPSR-v2 cultured mNPCs reached 80-90% confluence in 2D culture, cells were dissociated into single cells using Accumax Cell Dissociation Solution. 30,000 cells were seeded into each well of U-bottom 96-well plate with 100 μ l mNPSR-v2 medium and cultured overnight for re-aggregation. On the next day (Day 0), spinal cord was isolated from E12.5 embryo, and 3D mNPC aggregates were transferred to 6-well format transwell membrane tightly close to spinal cord dorsal part with 1.2mL KR5 in bottom well. Medium was changed every other day with fresh KR5 medium, and the samples were harvested for various assays on day 7.

Mouse engineered kidney generation from cultured NPCs and UB

Mouse UB (mUB) was cultured as we previously described⁴. The day before mouse kidney reconstruction, mNPCs were dissociated and 50,000 cells were seeded into one well of U-bottom 96-well low-attachment plate with 100 μ L mNPSR-v2 medium and cultured overnight in 37°C incubator to generate 3D mNPC aggregate. A small piece (with 6-10 branching tips) of day 5-10 cultured mUB organoid was manually dissected out using sterile needles and inserted into a microdissected hole in a 3D mNPC aggregate (sterile needle was used to pierce a hole in the center of mNPC aggregate sphere). This structure was then transferred into a well of a U-bottom 96-well low-attachment plate with 100 μ l kidney reconstruction medium (APEL2 + 0.1 μ M TTNPB) plus 10 μ M Y27632, using a P200 pipette with the top 0.5-1 cm of the tip cut to widen the tip, and cultured in 37°C incubator (day 0). After 24 h (day 1), the reconstructed UB/NPC structure was then transferred onto a 12-well transwell insert membrane (Corning, Cat. No. 3460). 300 μ l kidney reconstruction medium was added to the lower chamber of the transwell. Medium was changed

every two days for a total of 7 days while the reconstructed kidney branching and maturation progressed.

Chicken chorioallantoic membrane (CAM) assay

CAM assay was conducted as a cost-effective method to evaluate the nephrogenic potential of cultured NPCs *in vivo*. Briefly, Cas9-GFP mNPC lines were dissociated into single cells, and then 30,000 cells were seeded into 96-well U-bottom low-attachment plate (Thermo Fisher Scientific, # 174929) in mNPSR-v2 medium to generate 3D NPC aggregate. On the next day (D0), change medium with 100ul KR5-CF medium and follow by continuous two days culture (D0-D2). On day 2, transfer 3D NPC aggregates into chicken chorioallantoic membrane. On day 5 and day 7, use microscope to take videos to record the vasculature system in implants. On day 7, harvest the samples for various assays.

Dissociation of postnatal P3-P7 mouse kidneys and further culture in mNPSR-v2

P3-P7 pups were euthanized, and the kidneys were dissected. Mince one kidney into small pieces using blade (Cincinnati Surgical, # 75870-580). Collect small amount of kidney pieces into an Eppendorf tube (after spinning down, the pellet volume should be less than 30 μ l). Spin down at 300g for 5min, remove the supernatant and resuspend the pellet with 500 μ l warmed-up FRESH 1X Collagenase IV (Thermo Fisher Scientific, # 17104019). Put the Eppendorf tube into rotating shaker (Eppendorf ThermoMixer® F2.0) set at 37C with 800rpm shaking speed. Every 10min, take out the tube and pipet up and down the samples for 10 times. Dissociation in Col IV for a total of 30min. After 30min and the 3rd pipetting, spin the cells down at 300g for 1min to collect the kidney tubules and glomerulus as the pellet. Resuspend the pellet with warmed-up 500ul Accumax. Put the Eppendorf tube into rotating shaker set at 37C with 800rpm shaking speed. Every 10min, take out the tube and pipet up and down the samples for 10 times. Dissociation in Accumax a total of 30min. After 30min, add 500 μ l 10% FBS to neutralize the dissociation. Then

start the 3rd pipetting for 20 times. Spin down the cells at 300g for 5min, remove supernatant, and resuspend the pellet with 200 μ l ACK lysing buffer (Thermo Fisher Scientific, # A1049201), to remove the blood cells (room temperature for 3min). Add 1ml 10% FBS and spin the cells down at 300g for 5min. Remove the 1.2ml supernatant and resuspend the cells into 100 μ l 10% FBS medium for cell counting (use Trypan Blue to determine the live cell percentage). Usually, the live cell percentage of dissociated cells was 50-75%. Dissociated whole kidney cells were further cultured with mNPSR-v2 medium to induce *Six2*⁺ NPC-like cells. Note that for this culture, iMatrix-511 (Nacalai USA, # 892021), but not Matrigel, was used for coating plates, to enhance the attachment of the postnatal kidney cells to the plate.

Generation of *SIX2*-GFP/*PAX2*-mCherry knock-in dual reporter hPSC line

CRISPR-Cas9 based genome editing was used to insert 2A-EGFP-FRT-PGK-Neo-FRT or 2A-mCherry-loxP-PGK-Neo-loxP cassette downstream of the stop codon (removed) of endogenous *SIX2* or *PAX2* gene, respectively. DNA sequences ~1 kb upstream and ~1 kb downstream of the stop codon for endogenous *SIX2* (upstream F: CCGGAATTCTGCCAGTTGGAGCTACAG; upstream R: TACGAGCTCGGAGCCCAGGTCCACGAGGTT; downstream F: CGCGTCGACAACCCATTGCCTTGATGAG; downstream R: CCCAAGCTTCCCGAAGAACATTACATGAGG) or *PAX2* (upstream F: GAAGTCGACTTCCACCCATTAGGGGCCA; upstream R: TATGCTAGCGTGGCGGTATAGGCAGCGG; downstream F: TATAC-GCGTTACCGCGGGACCACATCA; downstream R: GACGGTACCACTGCTGGAG-GAAGAC) were cloned as homology arms upstream and downstream of 2A-EGFP-FRT-PGK-Neo-FRT (for *SIX2*-GFP) or 2A-mCherry-loxP-PGK-Neo-loxP cassette (for *PAX2*-mCherry), respectively, to facilitate homologous recombination. 2A-EGFP fragment was cloned from pCAS9_GFP (Addgene # 44719) and the FRT-PGK-Neo-FRT cassette was cloned from pZero-FRT-Neo3R (kindly provided by Dr. Keiichiro Suzuki). 2A-mCherry-loxP-Neo-loxP fragment was

cloned from Nanog-2A-mCherry plasmid (Addgene # 59995). The different fragments were then cloned to a modified pUC19 plasmid with additional restriction sites inserted, to make the complete donor plasmids for both knock-in experiments. Oligos for making sgRNA-expressing plasmid for *SIX2* knockin (F: CACCGGGGCTCCTAGAACCCATTG; R: AAAC CAAATGGGTTCTAGGAGCCCC) or *PAX2* knockin (F: CACCGATGACCGCCACTAGTTACCG; R: AAACCGGTAACTAGTGGCGGTTCATC) were synthesized, annealed, and cloned into the pSpCas9(BB)-2A-Puro (PX459) V2.0 plasmid (Addgene # 62988). Both donor and sgRNA plasmids for *SIX2* reporter knockin were transfected into the H1 hESCs using the Lipofectamine 3000 Transfection Reagent (Invitrogen, Cat. No. L3000015). Neomycin-resistant single cell colonies were picked up manually and genotyping was performed based on PCR. Clones with biallelic knock-in of *SIX2*-GFP were chosen for second round screen where plasmid encoding flippase was delivered via transfection to allow the transient expression of flippase, whose activities excise the FRT-flanked PGK-Neo cassette from the *SIX2*-GFP knock-in alleles. PCR was performed to identify single cell clones in which PGK-Neo cassettes were excised from both alleles. Then the same strategy was used to knock in *PAX2* reporter based on the successful biallelic *SIX2*-GFP knock-in clones.

PKD2 knock-out in *SIX2*-GFP knock-in reporter hPSC line

SIX2-GFP knock-in reporter hPSC line was generated using the method described above. We further knocked out *PKD2* gene in the reporter hPSC line using CRISPR/Cas9 based genome editing. For that, sgRNA was designed to target the first exon of human *PKD2* gene with sgRNA targeting sequence: CCGCGATAACCCCGGCTTCG. sgRNA was inserted into lentiCRISPR v2 plasmid (Addgene # 52961) and lentivirus was produced and then infected into *SIX2*-GFP hPSC line. After puromycin selection followed by clonal expansion of hPSCs, 11 single cell clones were picked up and expanded. Proteins were extracted from the 11 single cell clones and Western blot was performed to identify the candidate *PKD2*^{-/-} clones #10 and #11. PCR-based genotyping from

the genomic DNA, following by Sanger sequencing, further confirmed the generation of frame-shift mutations in both alleles of *PKD2* gene from #10 and #11 clones.

Deriving iNPC lines from human pluripotent stem cells

Deriving iNPC lines from FACS-purified *SIX2*-EGFP/*PAX2*-mCherry iNPCs

Directed differentiation from *SIX2*-GFP/*PAX2*-mCherry knock-in dual reporter hPSCs into iNPCs was performed following a previously published protocol⁵, with minor modifications. Briefly, hPSCs were dissociated into single cells with Accumax and 40,000 cells were seeded into one well in a 12-well plate with 1ml mTeSR medium plus 10 µM Y27632. Medium was changed daily with fresh 1ml mTeSR medium without Y27632 for another 2 days. At this time (day 0), hPSCs formed small colonies and were ready for directed differentiation. Phase 1, day 0 to day 4 (D0-D4), hPSCs were cultured with 1 ml Advanced RPMI 1640 Medium (Thermo Fisher Scientific, # 12633-012) supplemented with 8 µM CHIR99021 and 10nM LDN193189; medium was refreshed on D2 and D3. Phase 2 (D4-D7), medium was changed to Advanced RPMI 1640 Medium supplemented with 10 µM Y27632 and 10 ng/ml activin A; medium was refreshed daily. Phase 3 (D7-D10), medium was changed to Advanced RPMI 1640 Medium supplemented with 50 ng/ml FGF9; medium was changed daily till D10. On D10, cells were dissociated into single cells with pre-warmed Accumax, and *SIX2*-GFP/*PAX2*-mCherry iNPCs were sorted out through BD FACSaria™ III Cell Sorter. Sorted iNPCs were counted and 10,000 cells were seeded into one well in a 96-well plated coated with Matrigel and cultured with 100 µl hNPSR-v2 medium (Table S12). The medium was refreshed 2 days after cell seeding. When iNPCs grew to 80-90% confluent (on day 3 or day 4), the culture medium was removed, and the cells were washed once with 100 µl PBS, and then dissociated with 50 µl pre-warmed Accumax. The cells were incubated with Accumax for 8 mins, and then 150 µl 10% FBS medium was added to neutralize Accumax. The medium was pipetted up and down GENTLY for 5-7 times to make single cell suspension, which was then seeded at 1:10 passage ratio to a new well in 96-well plate. Change medium 2

days after seeding. On day 3 or day 4, the cells grew to 80-90% confluent and can be passaged again using the same protocol described above. (Note, Matrigel coating protocol for iNPC culture is the same as the one described for mNPC culture.)

Deriving iNPC lines without prior FACS-based purification of iNPCs

hPSCs were differentiated following the same protocol described above to generate iNPCs. On D10 of differentiation, instead of using FACS to purify the iNPCs based on *SIX2*-GFP; *PAX2*-mCherry dual reporter system, the dissociated whole cells were counted and then 10,000 cells were seeded into one well of 96-well coated with Matrigel and cultured with 100 μ l hNPSR-v2 medium. Thereafter, after 2 weeks of continuous culture and passage in hNPSR-v2 medium following protocol described above, stable iNPC line was established with 90-95% purity of iNPCs.

Deriving single cell clonal iNPC lines

When iNPC lines are stably established, single cell clonal iNPC lines can be generated. For that, when the iNPC lines grew to around 80% confluence, the cells were dissociated into single cells following the protocol described above for passaging iNPCs. The cells were counted and seeded into Matrigel-coated 96-wells at the density 0.5 cell per well with 100 μ l hNPSR-v2 medium so that most wells would have either one single cell or no cell (day 0). On day 3, 50 μ l used medium was removed, and 100 μ l fresh medium was added. On day 6, the used medium was completely removed and 100 μ l fresh medium was added. On day 9, NPC clones were clearly observed under the microscope in about 30% of the wells seeded. Cells in these wells were dissociated following our protocol described above, and all the cells were seeded into another 96-well. On day 12-14, the cells reached around 80-90% confluence and were passaged routinely every 3 or 4 days at the ratio of 1:10 as described above for bulk iNPC culture. To determine cloning efficiency, 60 wells of a 96-well plate were seeded with single cell NPC following the method mentioned above (D0). On day 3, the wells containing clusters of cells from a single cell were

labeled and counted, and the wells without any cell were discontinued. On day 9, the number of wells grown at least 40% confluence was counted. Cloning efficiency was calculated by using the number of wells recorded on day 9 divided by the number of wells recorded on day 3, from three independent experiments.

Deriving hNPC lines from human fetal kidneys

Tweezers were utilized to dissect nephrogenic zones from 9 to 12 week-old human fetal kidneys. Nephrogenic zones were minced into small pieces, and transferred into 1.5 mL Eppendorf tubes, and spun down at 300 g for 3 minutes. (Note that we aliquoted the kidney pieces into multiple tubes to ensure the volume of the tissue pellet after centrifugation was less than 100 μ l per tube to ensure best dissociation). The dissection medium was then carefully aspirated. The kidney pieces were then washed once with sterile PBS. 500 μ L of pre-warmed Accumax was added to the tube to resuspend the kidney pieces. The tube was incubated in 37°C incubator for 20~22 minutes. 500 μ L 10% FBS medium (10% FBS in DMEM) was added to the tube, and then GENTLY pipetted up and down 20 to 25 times to further dissociate the kidney pieces. The tube was spun down and the supernatant was then removed. FACS medium (cold PBS with 2% FBS) was added to resuspend the cell pellet and the cell suspension was filtered through 40 μ m cell strainer (Greiner bio-one, Cat. No. 542040) to remove cell clumps. Cells were counted and diluted to 1 million cells per 100 μ l in FACS medium, and ITGA8 antibody (R&D Systems, # AF4076) was added at the ratio of 1:200 for live cell staining. The incubation with ITGA8 antibody was performed on ice for 1 hour, followed by wash with 1 ml FACS medium and incubation for 1 hour with fluorescence protein-conjugated secondary antibody (Donkey anti-Goat IgG (H+L) Highly Cross-Adsorbed Secondary Antibody, Alexa Fluor Plus 488 or 568, Thermo Scientific, # A11055 or A11057) protected from light. After that, another wash with 1 ml FACS medium was performed and the cell suspension was then subjected to FACS to sort out ITGA8 $^{+}$ hNPC through BD FACSaria™ III Cell Sorter. Purified ITGA8 $^{+}$ hNPCs (70-90% SIX2 $^{+}$ /PAX2 $^{+}$) were cultured with the

same protocol as described for purified *SIX2*-GFP; *PAX2*-mCherry iNPCs. After 2 to 3 passages in hNPSR-v2 medium, stable hNPC line with 90-95% hNPCs were established.

Lentiviral expression of mCherry in iNPCs

30,000 *SIX2*-GFP⁺/*PAX2*-mCherry⁺ iNPCs were seeded into one well in 24-well plate. 24 hours later, iNPCs were infected with lentivirus expressing mCherry driven by EF1 α promoter (EF1a_mCherry_P2A_Hygro, Addgene, # 135003) using spinfection method described above. 24 hours after infection, 150 μ g/ml Hygromycin B (Thermo Scientific, Cat. No. 10687010) was added to the medium to select for iNPCs that have been successfully infected. More than 95% of the iNPCs showed bright mCherry expression after 1 week of Hygromycin B selection. (Note that exogenous mCherry is much brighter than endogenous mCherry from the *PAX2*-mCherry reporter, allowing the separation of these two mCherry signals.)

Targeted genome editing at the *AAVS1* loci in iNPCs

30,000 *SIX2*-GFP⁺/*PAX2*-mCherry⁺ iNPCs were seeded into one well in 24-well plate. 24 hours later, iNPCs were transfected with a mixture of two plasmids that provide donor DNA for targeted knockin of CAG promoter-driven mCherry expression cassette at the *AAVS1* loci (pAAVS1-P-CAG-mCherry, Addgene, # 80492), and that express Cas9 and sgRNA (pXAT2, Addgene, # 80494), at the ratio of 3:1, using Lipofectamine 3000 transfection reagent. 24 hours after transfection, 0.3 μ g/ml puromycin was added to the medium to select for iNPCs that have been successfully gene edited. More than 97% of iNPCs showed bright mCherry expression after 1 week of puromycin selection. (Note that exogenous mCherry is much brighter than endogenous mCherry from the *PAX2*-mCherry reporter, allowing the separation of these two mCherry signals.)

Generation of human nephron organoids from human NPC lines

iNPCs or hNPCs cultured in hNPSR-v2 medium were dissociated into single cells using Accumax as described above. 30,000 cells were seeded into one well of a U-bottom 96-well plate (Thermo Fisher Scientific, # 174929) and cultured with 100 μ l hNPSR-v2 medium overnight for cells to aggregate. On the next day (Day 0), 3D NPC aggregates were transferred onto 6-well format transwell membrane (Corning, # 3450) with 6 μ M CHIR99021 in 1.2 mL STEMdiff™ APEL™2 medium (STEMCELL Technologies, # 05270) at the bottom of the chamber for 1-hour. Then medium on the bottom chamber was removed as much as possible, and 1.2mL STEMdiff™ APEL™2 medium with 50 ng/mL FGF9 and 1 μ g/mL heparin was added for continuous culture. This medium was refreshed every other day. On Day 5, medium was changed to 1.2mL STEMdiff™ APEL™2 medium without any other factors. The medium was refreshed every other day till Day 14, when the samples were harvested for various assays.

Growth curve analysis of NPCs cultured in mNPSR-v2 or hNPSR-v2 media

For the growth curve analysis, 5,000 mNPCs, iNPCs, or hNPCs were seeded into each well of a 96-well plate coated with Matrigel and cultured in their corresponding mNPSR-v2 or hNPSR-v2 media. For each experiment, 16 wells were prepared for each line tested. Every 24 hours, 4 wells were dissociated, and the cell number was counted till 4 days after initial cell seeding, to determine the cell growth from day 0 to day 4. Three independent experiments were performed for each NPC line, serving as three biological replicates, to calculate the average cell numbers and the error bars at each time point.

Bulk RNA sequencing

Cultured mouse and human NPC samples were collected and lysed in TRIzol reagent or DNA/RNA Shield and stored at -80°C. Total RNA was extracted using Direct-zol RNA MicroPrep Kit (Zymo) or Quick-RNA Microprep Kit (Zymo). Bulk RNA-Sequencing was then performed through the Molecular Pathology Genomics Core of Children's Hospital Los Angeles (CHLA), or

through Novogene USA Inc. For sequencing through CHLA, cDNA library was prepared using KAPA Stranded mRNA-Seq Kit (KAPA Biosystems) and sequenced using Illumina HiSeq 2500. For sequencing through Novogene, library prep and sequencing were performed using standard Novogene bulk RNA-seq pipeline.

Bulk RNA-seq data analysis

RNA sequencing data was analyzed using Partek Flow Genomic Analysis Software. In addition to the new data generated from mouse and human NPC lines described in this study, legendary bulk RNA-seq data of primary mouse and human NPCs were used as positive controls, and primary kidney cells that are not NPCs were used as negative controls. These include E12.5 Six2-negative primary mouse non-NPCs, E11.5, E12.5, E13.5, E16.5 and P0 primary mouse NPCs¹, SIX2-negative primary human non-NPCs, SIX2+ human NPCs, SIX2+/MEIS1+ human NPCs,⁶ and ITGA8+ human NPCs³. FASTQ files were trimmed from both ends based on a minimum read length of 25 bps and an end minimum quality score (Phred) of 20 or higher. For mouse samples, reads were aligned to mm39 using STAR 2.7.8a. For human samples, reads were aligned to hg38 using STAR 2.7.8a. Aligned reads were quantified to the Partek E/M annotation model. Gene counts were normalized using DESeq2 Median ratio. DESeq2 Median ratio values can be found in Table S4 (mouse NPCs) and Table S13 (human NPCs). 972 mouse NPC signature genes were identified by comparing primary Six2⁺ E12.5 NPCs and primary Six2⁻ E12.5 non-NPCs¹, with cutoff of fold change > 1.5 or < -1.5, and p-value < 0.01 using DESeq2 (Table S4). 1058 human NPC signature genes were identified by comparing 5 datasets of primary ITGA8⁺, SIX2⁺ or SIX2⁺/MEIS1⁺ NPCs with 2 datasets of primary SIX2⁻ non-NPCs^{2,3}, with cutoff of fold change > 1.5 or < -1.5, and FDR < 0.05 using DESeq2 (Table S13). Principle component analysis (PCA) was performed using the mouse or human NPC signature genes identified. Hierarchical clustering of selected genes was produced based on the genes' DESeq2 Median

ratio values, clustering samples and features with average linkage cluster distance and Euclidean point distance.

Genome-wide CRISPR screen

The Brie genome-wide CRISPR knockout library⁷ (Addgene # 73632) was introduced to cultured NPCs via lentiviral infection in two different NPC lines as two biological replicates. This library contains 4 sgRNAs for each of the 19,674 protein-coding genes of the mouse genome, and 1,000 non-targeting control sgRNAs, totaling 78,637 unique sgRNAs (Table S5). The infection was carried out at a low multiplicity of infection (MOI) of 0.3, to ensure the majority of the NPCs express only one sgRNA. For each experiment, twenty-five million NPCs were used for the initial infection so that at least 100 cells would carry the same sgRNA to protect against random loss of sgRNA if lower cell number was used. 0.3 µg/ml puromycin was added 48 hours after lentiviral infection, to select for the successfully infected cells, which were further cultured continuously for a total of 3 weeks since lentiviral infection. Genomic DNA was extracted after 3 weeks of culture, and targeted PCR was performed to amplify the sgRNA integrated into the genome for next-generation sequencing, following Sequencing Protocol provided by Addgene (“Broad Institute PCR of sgRNAs for Illumina sequencing”). Next-generation sequencing was performed from the Molecular Pathology Genomics Core of Children’s Hospital Los Angeles using Illumina HighSeq 2500.

Genome-wide CRISPR screen data analysis

Normalized read counts for each individual sgRNA in the plasmid library, before and after CRISPR screen (Table S5), CRISPR screen beta scores (Table S6), and the scatterplots of beta scores, were generated using MAGeCKFlute⁸. 1798 genes from CRISPR screen replicate #1, and 1627 genes from CRISPR screen replicate #2, with beta scores > 1.5 or < -1.5, and p-values < 0.05, were identified as potential hits (Table S7) for further analyses using Canonical Pathway Analysis

tools of the Ingenuity Pathway Analysis (IPA) platform (Table S8). Full list of reference FGF, Wnt, and LIF signaling pathway-related genes, and the genes identified in the screens, were summarized in Table S9. Full list of NPC-specific genes identified by comparisons between primary E12.5 NPC and primary E12.5 non-NPC¹, or between primary E16.5 NPC and primary E16.5 IPC², and the 64 highly confident NPC self-renewal hits, were summarized in Table S10. Full list of reference CAKUT or Wilms tumor-related genes, and the genes identified in the screens, were summarized in Table S11.

KMT2A and KAT6A inhibitor treatment experiments

20,000 mNPCs were seeded into each Matrigel-coated well of 96-well plates, and cultured in (1) mNPSR-v2 + DMSO, (2) mNPSR-v2 + 100 nM WDR5 degrader, (3) mNPSR-v2 + 1 µM MLL1 (inh), (4) mNPSR-v2 + 5 µM MOZ-IN-3, or (5) mNPSR-v2 + 5 µM WM-1119. Medium was changed every two days and samples were harvested for immunofluorescence staining and qRT-PCR assay on day 8. Three independent experiments were conducted for each group as biological replicates.

Establishment of one-step multiplexed CRISPR/Cas9 knockout lentiviral plasmids

Three different sgRNAs (sgRNA-A, sgRNA-B, and sgRNA-C) were designed to target *EGFP* coding sequences⁹, or the first exons of *Pkd1*, or *Pkd2* genes. These sgRNAs were inserted individually into lentiGuide-Puro plasmid (Addgene # 52963) following the cloning protocols provided from the plasmid depositor. Then, for each target gene, the three sgRNA expression cassettes were subcloned one by one from the three lentiGuide-Puro plasmids into a modified pLKO.1-TRC plasmid (additional multiple cloning site BclI-EsrGI-Mlul-Nhel-PstI-Sall-XbaI-XmaI was inserted between the original PpuMI and EcoRI sites in the pLKO.1-TRC plasmid (Addgene # 10878)) to make tandem sgRNA expression cassettes in the same lentiviral vector.

sgRNA targeting sequences:

Gene	sgRNA-A	sgRNA-B	sgRNA-C
<i>EGFP</i>	AAGGGCGAGGAGCTGTTCAC	CTGAAGTTCATCTGCACCAC	GGAGCGCACCATCTTCTCA
<i>Pkd1</i>	GCTGCGCTGACGATGCCGCT	CTGGCCGGAGACCCTGGGCG	AGCGGCCGGAGCAATTGACG
<i>Pkd2</i>	CGAGATGGAGCGCATCCGGC	TCGCCCCGCGCCGCGAGCGTC	AGTGGCGCCGGGCAGTCGG

One-step gene knockout in mouse NPCs with multiplexed CRISPR/Cas9 KO system

Multiplexed CRISPR/Cas9 KO plasmids targeting *EGFP*, *Pkd1*, or *Pkd2* were generated as described above. Lentivirus was produced from these plasmids and used to infect mNPCs. For that, lentivirus was first packaged following protocols we described previously¹ and was then concentrated 100x using Lenti-X Concentrator kit (Takara, # 631231). Concentrated lentivirus was aliquoted and stored in -80°C before use. The lentivirus was used at 1x final concentration together with 10 µg/ml polybrene (Sigma-Aldrich, Cat. No. TR-1003-G) diluted in mNPSR-v2. Lentiviral infection was conducted in mNPC cultured in wells of 96-well plate. (1) For gene editing in Cas9-EGFP mNPC line, used culture medium was removed from each well and 100 µl lentivirus-polybrene-mNPSR-v2 mixture was added to the well. The plate was then centrifuged at 800 g for 15 minutes at room temperature. After the spinfection, the lentivirus-polybrene-mNPSR-v2 mixture was removed and the infected mNPCs were washed three times gently with 150-200 µl pre-warmed PBS, then cultured in 100 µl fresh mNPSR-v2 medium. 24 hours after infection, 0.3 µg/ml puromycin was added to the medium to select for NPCs that have been successfully infected. (2) For gene editing in *Six2*-GFP mNPC lines or wildtype mNPC lines cultured in 96-well plate, cells were first infected with lentivirus containing lentiCas9-Blast plasmid (Addgene, # 52962) using similar spinfection protocol described above. 24 hours after infection, 2 µg/ml blasticidin was added to the medium to select for NPCs that have been successfully infected. 1 week after selection, these Cas9-expressing mNPCs were infected with lentivirus expressing multiplexed CRISPR/Cas9 KO system as described above to generate gene KO starting from the

wild-type mNPC line. Once bulk *Pkd1*^{-/-} or *Pkd2*^{-/-} mNPC lines were generated, single cell clonal *Pkd1*^{-/-} or *Pkd2*^{-/-} mNPC lines were generated following the same protocols we described above for generating clonal mNPC lines from mNPCs.

Genotyping of *Pkd1*^{-/-} or *Pkd2*^{-/-} single cell clonal mNPC lines

Genomic DNA of *Pkd1*^{-/-} or *Pkd2*^{-/-} single cell clonal mNPC lines were extracted using QuickExtractTM DNA Extraction Solution (Lucigen, # QE09050). PCR primers were designed to flank the sgRNA targeting sites of *Pkd1* or *Pkd2* genes (listed below). PCR were performed and PCR amplicons were used to conduct gel running and purified by DNA Clean & Concentrator kit (Zymo Research, # D4031). A-tailing were then performed on the purified PCR products following the NEB protocol: <https://www.neb.com/protocols/2013/11/01/a-tailing-with-taq-polymerase>. A-tailed PCR products were ligated with digested linear pGEM[®]-T Vector (Promega, Cat. No. A3600), followed by transformation with One ShotTM TOP10 Chemically Competent E. coli (Thermo Fisher Scientific, # C404010). Transformed E. coli were evenly daubed on IPTG/X-gal/Amp agarose plates and incubated at 37°C overnight. White bacterial clones were then picked up, inoculated, followed by mini-prep plasmid extraction (Zymo Research, # D4020). Extracted plasmids were sent to for Sanger sequencing. SnapGene software was utilized to analyze sequencing data.

Primers for PCR-based *Pkd1*^{-/-} or *Pkd2*^{-/-} genotyping:

Gene	Forward	Reverse
<i>Pkd1</i>	CCCTCCTGAAC TGCGGCT	GGACCCAGTCATGATGCTCTA
<i>Pkd2</i>	GCAAGCTACCCCGTAGGAATG	GCGCAGGCAGTTGTCAAGC

Optimization of mini *Pkd2*^{-/-} cystic organoid generation

Clonal *Pkd2*^{-/-} mNPC lines and *GFP*⁺ mNPC lines were used to optimize mini organoids model. For the first round of optimization, after mNPSR-v2 cultured NPCs reached 80-90% confluency in 2D culture, cells were dissociated into single cells using Accumax Cell Dissociation Solution. 500,000 cells were seeded into each well of AggreWell™800 24-well Plate (STEMCELL Technologies, Cat. No. 34850) with 2 mL mNPSR-v2 medium and cultured overnight. On the next day (Day 0), mini 3D NPC aggregates formed, and they were transferred into 12-well plates with around 30 mini aggregates/well in 1mL medium. mini 3D NPC aggregates were treated with different concentrations of CHIR99021 at 3.0 μ M, 4.5 μ M or 6.0 μ M in KR5 or hBI medium under shaking culture at 120 rpm (VWR Orbital Shaker Model 1000) for 2 days (D0-D2), and then followed by culture with KR5 or hBI for 5 days (D2-D7). For the second round of optimization, mini 3D NPC aggregates were transferred into 12-well plates or ultra-low attachment plates under shaking culture or suspension culture, and treated with CHIR99021 at 4.5 μ M in KR5 medium with 1% MTG or without MTG for 2 days (D0-D2), and then followed by culture in KR5 with 1% MTG or without MTG for 5 days (D2-D7). Cystic organoid formation efficiency was quantified based on 3-4 independent experiments and cyst diameters were measured by the measure tools of Olympus Cellsens Standard software. See also Figure S6 for more information.

hBI medium

Basal medium: DMEM/F12 (1:1) (1X), Invitrogen, Cat. No. 11330-032.

Supplements:

Reagent Name	Company	Cat. No.	Final Concentration
GlutaMAX-I (100X)	Invitrogen	35050-079	1X
MEM NEAA (100X)	Invitrogen	11140-050	1X
2-Mercaptoethanol (55mM)	Invitrogen	21985-023	0.1 μ M

Pen Strep (100X)	Invitrogen	15140-122	1X
B-27 Supplement (50X), minus vitamin A	Invitrogen	12587-010	1X
ITS Liquid Media Supplement (100×)	Sigma	I3146-5ML	1X

Generation of PKD organoid models from mouse and human NPC lines

Traditional PKD organoid models:

Clonal *Pkd2*^{-/-} mNPC lines or *PKD2*^{-/-} iNPC lines were used to generate corresponding mouse or human ADPKD models. The protocols for generation of mouse and human nephron organoids on transwell plates from NPC lines were described above. On day 7 (mouse) or day 14 (human) of organoid differentiation, each organoid was cut into 6 pieces using needles and subjected to shaking culture at 120 rpm (VWR Orbital Shaker Model 1000) in KR5 medium to develop cysts. Cystic organoid formation efficiency was quantified based on 3-4 independent experiments and cyst diameters were measured by the measure tools of Olympus Cellsens Standard software. For drug testing using this traditional PKD organoid model, for each drug treatment group, 30 small organoid pieces from fully developed mouse or human nephron organoids were pooled together in one well of a 12-well plate, cultured in KR5 medium with shaking, and supplemented with the drug to be tested. Drugs were freshly added to the medium and were refreshed with KR5 medium every two days. 4 days after drug treatment, cystic organoids were recorded through imaging and cyst formation efficiency and cyst diameter were quantified. Concentrations of drugs used in this study were determined based on previous publications ¹⁰⁻¹³. Cystic organoid formation efficiency was quantified based on 3-4 independent experiments and cyst diameters were measured by the measure tools of Olympus Cellsens Standard software.

Scalable mini PKD organoid models:

Clonal *Pkd2*^{-/-} mNPC lines or *PKD2*^{-/-} iNPC lines were used to generate corresponding mouse or human ADPKD mini organoid models. For that, 500,000 mNPCs or iNPCs were seeded into each

well of AggreWell™ 800 24-well Plate (STEMCELL Technologies, # 34850) with 2 mL mNPSR-v2 medium (mouse) or hNPSR-v2 medium (human), and cultured overnight to form mini aggregates (~300 mini aggregates per well, or ~7,200 mini aggregates per plate). On the next day (Day 0), mini 3D NPC aggregates from one well were transferred into 2 wells of 6-well plate with 2.5 mL KR5-CF medium in each well with shaking at 120 rpm. These aggregates were treated with KR5-CF medium for 2 days (mouse) or 3 days (human), then the medium was changed to 2.5 mL KR5 medium with medium refreshed every other day till harvested. Obvious PKD cysts typically emerged 4 days (mouse) or 8 days (human) after shaking culture. Cystic organoid formation efficiency was quantified based on 3-4 independent experiments and cyst diameters were measured by the measure tools of Olympus Cellsens Standard software.

Drug screening with scalable mini PKD organoid models

Commercially available small molecule library (Cayman, # 11076) targeting major epigenetic processes was used for drug screening in the scalable mini PKD organoid models. Following protocols described above, thousands of mini NPC aggregates were generated using a full plate of AggreWell™ 800 24-well Plate starting from 12 million *Pkd2*^{-/-} clonal NPC line #4, or #5, as two biological replicates. These mini NPC aggregates were seeded into 12-well plates with around 30 mini NPC aggregates per well (Day 0). These plates were then subjected to shaking culture with 1 mL KR5-CF medium per well for 2 days. Medium was changed to 1 mL KR5 medium per well after 2 days (Day 2). On Day 3, small molecules from the epigenetic library were added individually into each well at the concentration of 1 μ M, with controls that have DMSO, or different concentrations of metformin or tolvaptan. Cystic organoid percentages and cyst diameters were quantified on Day 5 as described above. Similar protocols were used when individual hits were further validated rather than from the initial screen. For drug testing in the human mini PKD organoid models, the KR5-CF step was extended to 3 days (Day 0 to Day 3), followed by KR5 step with medium refreshed every two days. Drug candidates were added on Day 6, and data

were analyzed on Day 8. Cystic organoid formation efficiency was quantified based on 3-4 independent experiments and cyst diameters were measured by the measure tools of Olympus Cellsens Standard software.

Seahorse assays on *GFP*^{-/-} or *Pkd2*^{-/-} NPCs and *GFP*^{-/-} or *Pkd2*^{-/-} nephron organoids

The XFp Extracellular Flux Analyzer (Agilent) was used for extracellular flux measurements. For *GFP*^{-/-} mNPCs vs *Pkd2*^{-/-} mNPCs, 20,000 cells per well were seeded in iMatrix-511 (Nacalai USA, # 892021) coated Seahorse miniplates 18-20 hours before the assay. For *GFP*^{-/-} nephron organoids vs *Pkd2*^{-/-} nephron organoids, on Day 4 of shaking culture following the mini PKD organoid protocol, one single nephron organoid was seeded into each well of poly-L-lysine coated Seahorse miniplate 1 hour before the assay. The XF sensor cartridges were hydrated overnight at 37°C without carbon dioxide in the Seahorse XF calibrant solution, as recommended by the manufacturer protocol. For the cell energy phenotype test, cell culture medium was replaced with XF assay medium (unbuffered DMEM [pH7.4] with 17.5 mM glucose, 0.5 mM pyruvate, and 4.5 mM glutamine). Microplate with cells was placed in a 37°C incubator without carbon dioxide for one hour. Oligomycin and FCCP were added to the ports at the final concentration of 1 µM. Standard XFp cell energy phenotype test (3 cycles of baseline measurements and 5 cycles of Oligomycin + FCCP with 3 minutes mixing and 3 minutes measuring) were performed for 1hour. Measurements were recorded from three to six independent experiments with three technical replicates per group in each independent experiment. Data were either normalized to cell numbers for NPCs (stained and counted with Hoechst 33342), or normalized to total genomic DNA amounts for organoids (CyQUANT® Cell Proliferation Assay, Invitrogen, C7026). Data were analyzed using Wave software.

Immunofluorescence staining

Whole-mount staining:

Samples were fixed in 4% PFA (4% Paraformaldehyde Aqueous Solution, Electron Microscopy Sciences, #157-4) for 15 minutes (kidney organoids, cystic organoids, or engineered kidneys) in Eppendorf tubes or tissue culture plates at room temperature. They were then washed four times in 1X PBS (Corning, Cat. No. 21-040-CV) for total 30 minutes. After the washes, samples were blocked in blocking solution (0.3% PBST containing 3% BSA) for 30 minutes at room temperature or 4°C overnight followed by primary antibody staining (primary antibodies were diluted in blocking solution) at 4°C overnight. On the second day, samples were washed four times with 0.3% PBST for total 60 minutes at room temperature. Secondary antibodies diluted in blocking solution were added and samples were incubated at 4°C overnight. On the third day, samples were washed four times with 0.3% PBST for total 60 minutes at room temperature then mounted for imaging. Confocal Microscope Zeiss LSM 800: AxioObserver.M2 was used for imaging recording in this study.

Cryo-section staining:

Samples were fixed in 4% PFA for 30 minutes (human fetal kidneys, mouse embryonic kidneys, or mouse postnatal kidneys) in Eppendorf tubes or tissue culture plates at room temperature and then washed four times in 1X PBS for total 30 minutes. Fixed kidneys were transferred and incubated in 30% sucrose overnight at 4°C. After these kidneys sunk to the bottom in the sucrose on the next day, they were then transferred into a plastic mold and embedded in OCT Compound (Scigen, Cat. No. 4586K1) and froze in -80°C for 24 hours to make a cryo-block. The cryo-blocks were sectioned using Leica CM1800 Cryostat. For staining, these sectioned slides were blocked with blocking solution for 30 minutes followed by 2 hours of primary antibodies staining, all at room temperature. After primary staining, wash the slides four times with 0.3% PBST for a total of 15 minutes, then secondary staining for one hour at room temperature. After secondary staining, the slides were washed four times with 0.3% PBST for a total of 15 minutes and mounted with

mounting medium (Southern Biotech, Fluoromount-G® Mounting Medium, #0100-01). For the Cryo-section staining of human fetal kidneys and mouse embryonic kidneys with p-p38, p-Smad2 or p-Smad1/5/9 antibodies, we used TSA-based immunocytofluorescence staining with TSA Plus Cyanine 3 Evaluation Kit (PerkinElmer, # NEL744E001KT) to enhance the phosphorylation signals. Slides were first incubated with 3% H₂O₂ reagent at room temperature for 10 minutes, rinsed with PBS, then blocked for 30 mins with blocking buffer. After blocking, these slides were incubated with diluted primary antibody overnight at 4°C (p-Smad2 dilution ratio-1:4000, p-Smad1/5/9 dilution ratio-1:4000, p-p38 dilution ratio-1:8000, in blocking buffer). On the second day, slides were rinsed with 0.3% PBST, incubated with anti-rabbit or anti-mouse HRP (1:2,000 in blocking buffer) for 2 hours at room temperature, rinsed again with 0.3% PBST, then incubated with TSA working solution (1:100 dilution) for 15 minutes at room temperature followed by a final rinse with 0.3% PBST. After the completion of TSA-based staining, proceed to standard IF staining.

Immunofluorescence staining in 96-well plates:

NPCs cultured in 96-well plates were stained directly in the plates to determine various NPC marker gene expression. For that, the used culture medium was first removed from each well and 50 µl 4% PFA was added to fix the samples in the plates for 10 minutes at room temperature. Fixed samples were then gently washed three times in 1X PBS (Corning, Cat. No. 21-040-CV) 3 times for total 15 minutes, blocked in 100 µl blocking solution (0.1% PBST containing 3% BSA) for 30 minutes at room temperature, then followed by primary antibody staining at room temperature for 2 hours. Then, samples were gently washed two times with PBST for 10 minutes and secondary staining was conducted for one hour at room temperature. After the secondary staining, samples were gently washed three times with PBST for 15 minutes, and the PBST from the last wash was kept in the well to prevent samples from drying out. Samples were then ready for observation and recording. Note: NPCs cultured on Matrigel-coated 96-well plates can easily

detach from the plate during staining, it is important to add/remove reagents gently in the process of staining. Validated primary antibodies in this study can be found in “Key Resources Table”.

Imaging data quantification:

For immunostaining quantification, 3-4 different fields of view were randomly selected to count the number of positively stained cell numbers and total cell numbers (as determined by DAPI signals). At least 500 cells per field of view were included. Error bars represent standard derivation between different fields of views.

RNA isolation, reverse transcription, qRT-PCR, and immunoblotting

Samples were dissolved in 100 μ l TRIzol (Invitrogen, Cat. No. 15596018) or 100 μ l DNA/RNA Shield (Zymo Research, Cat. No. R1100-50) and kept in -80°C freezer. RNA isolation was performed using the Direct-zol RNA MicroPrep Kit (Zymo Research, Cat. No. R2062) or Quick-RNA Microprep Kit (Zymo Research, Cat. No. R1051) according to the manufacturer’s instructions. Reverse transcription was performed using the iScript Reverse Transcription Supermix (Bio-Rad, Cat. No. 1708841) following the manufacturer’s instructions. qRT-PCR was performed using SsoAdvanced Universal SYBR® Green Supermix (Bio-Rad, Cat. No. 1725274) or AzuraView GreenFast qPCR Blue Mix LR (Azura Genomics, Cat. No. AZ-2320) and carried out on an Applied Biosystems Vii 7 RT-PCR system (Thermo Scientific P/N 4453552). Validated gene-specific primers in this study can be found in Table S14. Fold changes were calculated from ΔCt using Gapdh as a housekeeping gene as previously described¹⁴. Immunoblotting experiments were performed as described previously¹⁴.

FACS

Cells were dissociated/prepared as described above. FACS sorting was performed on a BD FACS Aria™ III Cell Sorter, operated by experienced core facility staff at USC Stem Cell's FACS core. Sorted cells were collected in 1.5 ml Eppendorf tubes with 500 μ l dissection medium on ice.

QUANTIFICATION AND STATISTICAL ANALYSIS

Data are presented as mean \pm SD from at least three biological replicates (n=3). Statistical significance was determined by two-tailed unpaired Student's t tests; ns, not significant; *, p<0.05; **, p<0.01; ***, p<0.001.

SUPPLEMENTAL REFERENCES:

1. Li, Z., Araoka, T., Wu, J., Liao, H.-K., Li, M., Lazo, M., Zhou, B., Sui, Y., Wu, M.-Z., and Tamura, I. (2016). 3D culture supports long-term expansion of mouse and human nephrogenic progenitors. *Cell stem cell* 19, 516-529.
2. Lindström, N.O., Guo, J., Kim, A.D., Tran, T., Guo, Q., De Sena Brandine, G., Ransick, A., Parvez, R.K., Thornton, M.E., Baskin, L., et al. (2018). Conserved and Divergent Features of Mesenchymal Progenitor Cell Types within the Cortical Nephrogenic Niche of the Human and Mouse Kidney. *J Am Soc Nephrol* 29, 806-824. 10.1681/ASN.2017080890.
3. O'Brien, L.L., Guo, Q., Lee, Y., Tran, T., Benazet, J.-D., Whitney, P.H., Valouev, A., and McMahon, A.P. (2016). Differential regulation of mouse and human nephron progenitors by the Six family of transcriptional regulators. *Development* 143, 595-608.
4. Zeng, Z., Huang, B., Parvez, R.K., Li, Y., Chen, J., Vonk, A.C., Thornton, M.E., Patel, T., Rutledge, E.A., and Kim, A.D. (2021). Generation of patterned kidney organoids that recapitulate the adult kidney collecting duct system from expandable ureteric bud progenitors. *Nature communications* 12, 1-15.
5. Morizane, R., Lam, A.Q., Freedman, B.S., Kishi, S., Valerius, M.T., and Bonventre, J.V. (2015). Nephron organoids derived from human pluripotent stem cells model kidney development and injury. *Nat Biotechnol* 33, 1193-1200. 10.1038/nbt.3392.
6. Lindström, N.O., Guo, J., Kim, A.D., Tran, T., Guo, Q., Brandine, G.D.S., Ransick, A., Parvez, R.K., Thornton, M.E., and Baskin, L. (2018). Conserved and divergent features of mesenchymal progenitor cell types within the cortical nephrogenic niche of the human and mouse kidney. *Journal of the American Society of Nephrology* 29, 806-824.
7. Doench, J.G., Fusi, N., Sullender, M., Hegde, M., Vaimberg, E.W., Donovan, K.F., Smith, I., Tothova, Z., Wilen, C., Orchard, R., et al. (2016). Optimized sgRNA design to maximize activity and minimize off-target effects of CRISPR-Cas9. *Nat Biotechnol* 34, 184-191. 10.1038/nbt.3437.

8. Wang, B., Wang, M., Zhang, W., Xiao, T., Chen, C.-H., Wu, A., Wu, F., Traugh, N., Wang, X., and Li, Z. (2019). Integrative analysis of pooled CRISPR genetic screens using MAGeCKFlute. *Nature protocols* **14**, 756-780.
9. Zuo, E., Cai, Y.J., Li, K., Wei, Y., Wang, B.A., Sun, Y., Liu, Z., Liu, J., Hu, X., Wei, W., et al. (2017). One-step generation of complete gene knockout mice and monkeys by CRISPR/Cas9-mediated gene editing with multiple sgRNAs. *Cell Res* **27**, 933-945. 10.1038/cr.2017.81.
10. Low, J.H., Li, P., Chew, E.G.Y., Zhou, B., Suzuki, K., Zhang, T., Lian, M.M., Liu, M., Aizawa, E., and Esteban, C.R. (2019). Generation of human PSC-derived kidney organoids with patterned nephron segments and a de novo vascular network. *Cell stem cell* **25**, 373-387. e379.
11. Tran, T., Song, C.J., Nguyen, T., Cheng, S.-Y., McMahon, J.A., Yang, R., Guo, Q., Der, B., Lindström, N.O., and Lin, D.C.-H. (2022). A scalable organoid model of human autosomal dominant polycystic kidney disease for disease mechanism and drug discovery. *Cell Stem Cell* **29**, 1083-1101. e1087.
12. Li, L.X., Fan, L.X., Zhou, J.X., Grantham, J.J., Calvet, J.P., Sage, J., and Li, X. (2017). Lysine methyltransferase SMYD2 promotes cyst growth in autosomal dominant polycystic kidney disease. *The Journal of clinical investigation* **127**, 2751-2764.
13. Takiar, V., Nishio, S., Seo-Mayer, P., King Jr, J.D., Li, H., Zhang, L., Karihaloo, A., Hallows, K.R., Somlo, S., and Caplan, M.J. (2011). Activating AMP-activated protein kinase (AMPK) slows renal cystogenesis. *Proceedings of the National Academy of Sciences* **108**, 2462-2467.
14. Huang, B., Wang, B., Lee, W.Y.-W., Leung, K.T., Li, X., Liu, Z., Chen, R., cheng Lin, J., Tsang, L.L., and Liu, B. (2019). KDM3A and KDM4C regulate mesenchymal stromal cell senescence and bone aging via condensin-mediated heterochromatin reorganization. *Iscience* **21**, 375-390.